JOURNAL OF GEOPHYSICAL RESEARCH, VOL. 114, F01015, doi:10.1029/2008JF001010, 2009

Erosional variability along the northwest Himalaya

Rasmus C. Thiede,[1,2,3] Todd A. Ehlers,[1] Bodo Bookhagen,[4,5] and Manfred R. Strecker[2]

Received 3 March 2008; revised 17 September 2008; accepted 20 October 2008; published 10 February 2009.

[1] Erosional exhumation and topography in mountain belts are temporally and spatially variable over million year timescales because of changes in both the location of deformation and climate. We investigate spatiotemporal variations in exhumation across a 150 × 250 km compartment of the NW Himalaya, India. Twenty-four new and 241 previously published apatite and zircon fission track and white mica $^{40}Ar/^{39}Ar$ ages are integrated with a 1-D numerical model to quantify rates and timing of exhumation alongstrike of several major structures in the Lesser, High, and Tethyan Himalaya. Analysis of thermochronometer data suggests major temporal variations in exhumation occurred in the early middle Miocene and at the Plio-Pleistocene transition. (1) Most notably, exhumation rates for the northern High Himalayan compartments were high (2–3 mm a^{-1}) between ~23–19 and ~3–0 Ma and low (0.5–0.7 mm a^{-1}) in between ~19–3 Ma. (2) Along the southern High Himalayan slopes, however, high exhumation rates of 1–2 mm a^{-1} existed since 11 Ma. (3) Our thermochronology data sets are poorly correlated with present-day rainfall, local relief, and specific stream power which may likely result from (1) a lack of sensitivity of changes in crustal cooling to spatial variations in erosion at high exhumation rates (>~1 mm a^{-1}), (2) spatiotemporal variation in erosion not mimicking the present-day topographic or climatic conditions, or (3) the thermochronometer samples in this region having cooled under topography that only weakly resembled the modern-day topography.

Citation: Thiede, R. C., T. A. Ehlers, B. Bookhagen, and M. R. Strecker (2009), Erosional variability along the northwest Himalaya, *J. Geophys. Res.*, *114*, F01015, doi:10.1029/2008JF001010.

1. Introduction

[2] Recent work has suggested that erosionally driven exhumation plays an important role in the deformation history of collisional orogens such as the Himalaya [e.g., *Beaumont et al.*, 2001; *Hodges et al.*, 2001; *Koons*, 1989; *Willett*, 1999; *Zeitler et al.*, 2001]. The interactions between spatial and temporal variations in tectonics and exhumation are related to several factors. First, in convergent orogens tectonics governs the influx of material by accretion. According to the critical wedge theory, as an orogen grows the accumulation of mass changes and influences the location of deformation [e.g., *Dahlen et al.*, 1984; *Davis et al.*, 1983]. Changes in the location of deformation will activate different structures and affect local topographic slopes and erosive processes. Second, climate affects the spatial distribution of erosion on a variety of timescales [e.g., *Bookhagen et al.*, 2005; *Molnar and England*, 1990; *Pratt-Sitaula et al.*, 2004; *Schaller and Ehlers*, 2006; *Zhang et al.*, 2001]. Spatial and temporal variations in climate can thus change the locus of exhumation by redistributing mass, and in turn change the location of deformation and surface uplift to maintain critical taper [e.g., *Beaumont et al.*, 2001; *Dahlen and Suppe*, 1988; *Hilley and Strecker*, 2004; *Hoth et al.*, 2006; *Koons*, 1989; *Reiners et al.*, 2003; *Whipple and Meade*, 2006; *Willett*, 1999]. In this study we quantify the spatial and temporal variations in long-term (10^6–10^7 years) exhumation across the front of the NW Himalaya and evaluate the tectonic and erosional mechanisms responsible for the observed variations.

[3] Crustal shortening, rock uplift and erosion have shaped the Himalayan orogen since the India-Eurasia collision ca. 55 Ma ago [e.g., *Garzanti et al.*, 1987; *Patriat and Achache*, 1984]. After a longer phase of crustal thickening and peak metamorphism, deformation processes changed significantly during the early Miocene, when a metamorphic, possibly partially molten midcrustal layer was extruded [*Beaumont et al.*, 2001; *Grujic et al.*, 1996]. During this event the High Himalayan Crystalline complex was thrust far to the south, onto the Lesser Himalaya [*Gansser*, 1964]. Since then, vigorous erosion has affected the uplifting mountain front as evidenced by thick foreland-basin sediment sequences as well as sediments stored in the Indus and Bengal fans [e.g., *Clift et al.*, 2002; *Copeland and Harrison*, 1990].

[1]Department of Geological Sciences, University of Michigan, Ann Arbor, Michigan, USA.
[2]Institut für Geowissenschaften, Universität Potsdam, Potsdam-Golm, Germany.
[3]Now at Geologisches Institut, ETH Zurich, Zurich, Switzerland.
[4]Geological and Enviromental Sciences Department, Stanford University, Stanford, California, USA.
[5]Now at Department of Geography, University of California Santa Barbara, California, USA.

0148-0227/09/2008JF001010$09.00

[4] Major knickpoints in longitudinal river profiles [*Seeber and Gornitz*, 1983], topographic discontinuities [*Wobus et al.*, 2003] and young cooling ages obtained from low-temperature thermochronology analysis in the High Himalaya (HH) [*Blythe et al.*, 2007; *Grujic et al.*, 2006; *Huntington et al.*, 2006; *Jain et al.*, 2000; *Lal et al.*, 1999; *Schlup et al.*, 2003; *Sorkhabi et al.*, 1996; *Thiede et al.*, 2004, 2005; *Vannay et al.*, 2004] 150 km north of the Himalayan mountain front suggest rapid rock uplift and exhumation over the last ~3 Ma. Several competing orogenic processes have been invoked to explain the ongoing rock uplift and exhumation of the HH. These include (1) a midcrustal ramp forcing rock uplift within the orogenic wedge [*Cattin and Avouac*, 2000; *Pandey et al.*, 1995], (2) surface breaking faults causing uplift at the base of the HH [e.g., *Hodges et al.*, 2004; *Wobus et al.*, 2003] in combination with recent reactivation of the Main Central Thrust System (MCT) [e.g., *Catlos et al.*, 1997; *Harrison et al.*, 1997; *Seeber and Gornitz*, 1983], and (3) uplift through thrust sheet stacking [e.g., *DeCelles et al.*, 1998; *Robinson et al.*, 2006] and/or duplex formation by underplating [*Bollinger et al.*, 2004]. What is common to all these models is that they require erosional removal of cover units. Consequently, this erosion lead to localized strain within the orogenic wedge and rock uplift far away from the orogenic front.

[5] Significant climate change has accompanied the tectonic evolution of the Himalaya. Most notably, the Indian monsoon developed in the Miocene and has extensively impacted the timing and distribution of precipitation across the Himalayan front. The timing of Indian monsoon development is not well constrained and still a matter of debate. The monsoon could have initiated as early as ~23 Ma [*Clift and Sun*, 2006], and certainly existed by ~12–10 Ma [*Dettman et al.*, 2001, 2003; *Rea*, 1993]. Several studies also suggest monsoon intensification between ~9 and 7 Ma [*Huyghe et al.*, 2005; *Kutzbach et al.*, 1993; *Quade et al.*, 1989]. More recently, orbitally forced worldwide climate fluctuations modulating monsoon intensity and probably enabling moisture entry by the Westerlies into the NW Himalaya likely developed in the last ~2.6 Ma [*Prell and Kutzbach*, 1992; *Zhisheng et al.*, 2001]. The degree to which the previous variations in deformation and climate have influenced the formation of the Himalaya is still actively debated. Previous studies have defined how orogen-scale variations in tectonics and climate affect deformation and erosion across large orogen perpendicular transects. However, the magnitude and frequency of change in exhumation rates, variations in rock uplift, and topographic growth on small ($\sim 10^2$ km) spatial scales alongstrike of orogens is less well known.

[6] In this study we quantify the spatial and temporal distribution of exhumation over timescales of 10^6–10^7 years along the southern Himalayan margin in NW India. The spatial distribution of a large database of thermochronometer cooling ages is used as a proxy for exhumation. We evaluate if the long-term trends in exhumation are correlated with modern observations of topography, structure, and climate using present-day rainfall, relief and specific stream power data. We present 24 new apatite fission track ages (AFT) linked to 241 previously published AFT (n = 122) and zircon fission track (ZFT) ages (n = 58), as well as $^{40}Ar/^{39}Ar$ white mica ($^{40}Ar/^{39}Ar$-wM) ages (n = 61) (Figure 1). Our study integrates previous and new work by evaluating spatial and temporal variations in exhumation within a 150 × 250 km segment in the NW Himalaya, covering parts of Garhwal, Kinnauer, Kulu, Lahaul and Spiti in NW India. A one-dimensional (1-D) advective thermal model is used to calculate exhumation rates for each thermochronometer system and compare the predicted exhumation rates to morphometric variations across the range front.

2. Geologic Setting

[7] The 2500-km-long and ~300-km-wide Himalayan arc forms the southern margin of the India – Eurasia collision zone and the Tibetan Plateau. Since the collision, continued convergence has been accommodated along major fault zones, such as the Southern Tibetan Detachment System (STDS) [*Burchfiel et al.*, 1992; *Burg and Chen*, 1984], Main Central Thrust System (MCT), the Main Boundary Thrust Fault (MBT), and the Main Himalayan Thrust with the Frontal Thrust fault (MFT) as its most southern continuation (Figure 1) [*Fuchs*, 1981; *Gansser*, 1964; *Hodges*, 2000; *Lefort*, 1975]. Crustal shortening, thickening and peak metamorphism were achieved during the Eocene and Oligocene [*Searle et al.*, 1999; *Vance and Harris*, 1999]. During early Miocene (~23 Ma) the onset of decompression [e.g., *Dezes et al.*, 1999; *Searle et al.*, 1999; *Vannay and Grasemann*, 2001] was accompanied by rock uplift and rapid extrusion of high-grade High Himalayan Crystalline (HHC) rocks. Deformation was accommodated by simultaneous displacement along the STDS in the hanging wall and MCT in the footwall [*Burchfiel et al.*, 1992; *Burg and Chen*, 1984]. It has been hypothesized that a lower-crustal channel flow at high temperatures (~700–800°C) is extruded in this region [*Beaumont et al.*, 2001; *Jamieson et al.*, 2004]. The low-temperature data, however, used in this study record near-surface cooling (<~400°C) and thus postdate the deep-seated, high-temperature history. Later deformation propagated south, from the MCT to the MBT by ~10–5 Ma [*DeCelles et al.*, 2001; *Huyghe et al.*, 2001; *Meigs et al.*, 1995], and most recently to the MFT [*Lavé and Avouac*, 2001]. Contemporaneously, an increasing number of units of the Lesser Himalaya were detached from the underthrust Indian continent and became incorporated into the Himalayan orogenic wedge, forming the Lesser Himalayan Crystalline (LHC). These crystalline nappes were stacked, achieved peak metamorphism, and were exhumed, forming the LH Duplex in middle Miocene (~11 Ma) [*Caddick et al.*, 2007; *DeCelles et al.*, 2001; *Srivastava and Mitra*, 1994]. Today, the southern front of the Himalaya is formed by the sub-Himalaya, where the Miocene foreland-basin sediments are uplifted by the MFT. By accommodating about ~20 mm a^{-1} of crustal shortening the Main Himalayan Thrust with the MFT to the south takes up a major proportion relative motion between the underthrusting Indian plate and the Himalaya [*Bilham et al.*, 1997; *Lavé and Avouac*, 2001; *Wang et al.*, 2001].

[8] Variable tectonic and climatic forces during the topographic evolution of the Himalaya have generated the three main tectonomorphic provinces: Lesser (LH), High or Greater (HH), and Tethyan Himalaya (TH). The TH is

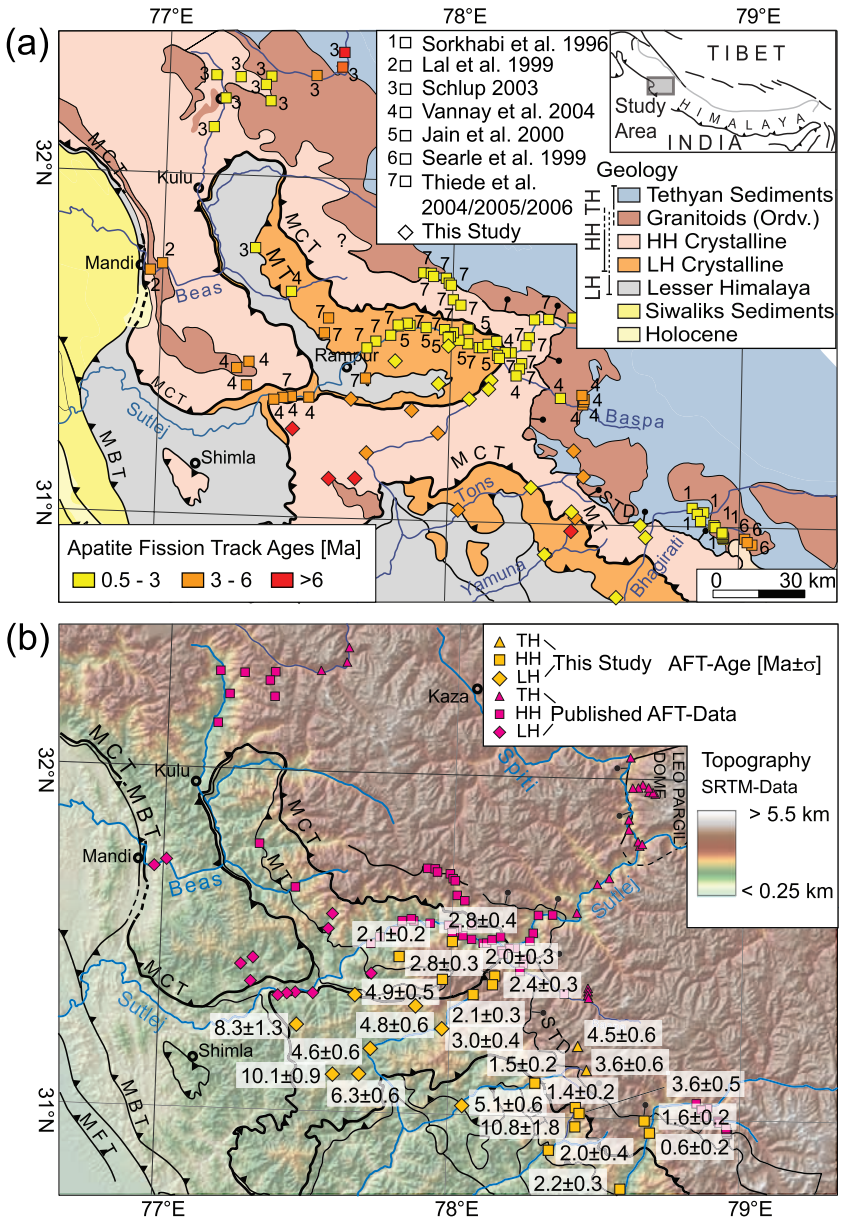

Figure 1. Spatial compilation of new and published apatite fission track (AFT) cooling ages across the southern Himalayan front, NW India, and used in this study. For zircon fission track (ZFT) and $^{40}Ar/^{39}Ar$-wM sample locations see Figure 5c; all thermochronology data used are listed in Table S2 in the data repository. (a) Sample locations with respect to the major tectono-morphic units and faults. Color coding of symbols refers to AFT cooling age in Ma. Diamond symbol denotes new analysis (Figure 1b shows the exact age), and squares identify published data with numbers corresponding to the publication. Orange symbols show location of the new analysis with the corresponding age and 1σ error. The different shape symbols represent tectono-morphic unit of the sample location, where triangles, squares, and diamonds correspond to Lesser, High, and Tethyan Himalaya, respectively. Notice in both Figures 1a and 1b the NW–SE striking belt of young (<3 Ma) AFT cooling ages along the transition between topographic Lesser Himalaya and High Himalaya. TH, Tethyan Himalaya; HH, High Himalaya; LH, Lesser Himalaya; STD, Southern Tibetan Detachment; MCT, Main Central Thrust; MT, Munsiari Thrust; MBT, Main Boundary Thrust; MFT, Main Frontal Thrust.

exposed north of the STDS and consists of Proterozoic to Eocene sedimentary rocks, which usually only show a low-grade metamorphic overprint [*Gaetani and Garzanti*, 1991]. The STDS separates the TH on top from the structurally underlying HHC. The HHC consists of high-grade metamorphic rocks and granitic intrusions, and forms the core of the mountain belt. The mylonites immediately below the MCT (in NW India also called the Vaikitra Thrust) separate the rocks of HHC from high-grade crystalline rocks related to the LHC below [*Ahmad et al.*, 2000; *Hodges et al.*, 1996;

Table 1. New Apatite Fission Track Data From the Sutlej/Garhwal Region[a]

Sample Number	Altitude (m)	Latitude (DD)	Longitude (DD)	Rock Type	Formation	Number of Individual Grains Dated	Spontaneous Rho-S	Spontaneous Ns	Induced Rho-I	Induced Ni	Dosimeter Rho-D	Dosimeter Nd	Chi-Square P (%)	Central Age Age (Ma)	Central Age Error ($\pm1\sigma$)	Dpar Microns	Dpar Error ($\pm\sigma$)	Dpar Number	Uranium (ppm)
RT05-98	1470	30.77094	78.59806	orthogneiss	LHC	20	0.322	51	25.119	3982	10.462	5104	19	2.2	0.4	2.33	0.19	63	29
RT05-102	2120	30.96067	78.69497	paragneiss	HHC	20	0.099	19	31.646	6078	12.454	5778	74	0.6	0.2	2.30	0.30	32	30
RT05-103	3390	30.99731	78.67617	paragneiss	HHC	21	0.337	68	44.315	8939	12.440	5778	26	1.6	0.2	2.27	0.26	71	41
RT05-106	1820	30.90525	78.35078	granite	MT	20	0.193	29	19.239	2896	12.425	5778	75	2.0	0.4	1.91	0.22	39	18
RT05-108	2620	30.97611	78.43967	orthogneiss	LHC?	30	0.322	46	6.077	868	12.411	5778	45	10.8	1.8	2.19	0.36	83	6
RT05-115	1170	31.03017	78.05072	granite	MT?	20	0.571	118	22.779	4708	12.368	5778	63	5.1	0.6	2.54	0.24	142	21
RT05-119	1510	31.19131	77.73281	Metasandst.	HHC?	19	0.707	101	30.939	4419	12.354	5778	56	4.6	0.6	2.36	0.28	98	31
RT05-120	2130	31.25503	77.97606	mica shist	HHC?	22	0.247	56	16.878	3834	12.340	5778	95	3.0	0.4	2.38	0.27	72	15
RT05-126	2390	31.34822	77.67533	orthogneiss	MT?	20	0.882	141	36.450	5828	12.326	5778	86	4.9	0.5	2.12	0.25	147	34
RT05-130	1970	31.46358	77.82275	orthogneiss	LHC	20	0.944	148	90.713	14221	12.297	5778	10	2.1	0.2	2.10	0.23	86	88
RT05-138	2660	31.25469	77.47714	paragneiss	HHC?	20	0.385	60	9.462	1476	12.283	5778	18	8.3	1.3	2.16	0.20	80	9
RT05-145	2970	31.51244	78.00392	orthogneiss	LHC	22	0.268	55	19.062	3912	12.254	5778	44	2.8	0.4	2.05	0.21	64	19
RT05-155	4710	31.39950	77.97444	orthogneiss	LHC	20	0.714	126	47.251	8338	11.283	5104	17	2.8	0.3	2.15	0.25	119	48
RT05-163	2350	31.32044	77.88408	paragneiss	HHC	15	0.787	79	30.114	3021	11.214	5104	43	4.8	0.6	2.88	0.27	107	34
RT05-167	3480	31.35808	78.08064	paragneiss	HHC	18	0.420	63	39.380	5901	11.146	5104	19	2.1	0.3	2.50	0.25	72	40
RT05-169	4580	31.38750	78.14572	paragneiss	HHC	24	0.369	67	28.488	5166	11.078	5104	69	2.4	0.3	2.80	0.29	68	29
RT05-170	3680	31.41442	78.15289	paragneiss	HHC	20	0.547	86	50.147	7886	11.009	5104	28	2.0	0.3	2.48	0.32	77	51
RT05-177	2340	31.10194	78.29928	orthogneiss	MCT?	20	0.334	52	39.346	6126	10.941	5104	86	1.5	0.2	2.37	0.26	67	42
RT05-184	3960	31.13747	78.47758	paragneiss	HHC	20	0.765	116	37.605	5701	10.873	5104	73	3.6	0.4	2.85	0.33	108	41
RT05-186	4430	31.21217	78.44289	granite	HHC	29	0.471	85	18.731	3382	10.804	5104	51	4.5	0.6	2.80	0.29	68	20
RT05-195	4940	31.03175	78.44006	paragneiss	HHC	20	0.368	53	46.178	6645	10.736	5104	51	1.4	0.2	3.05	0.27	90	49
RT05-197	4260	31.01539	78.45269	orthogneiss	HHC	24	0.246	60	11.933	2913	10.667	5104	55	3.6	0.6	2.46	0.29	75	12
RT05-202	1830	31.11547	77.69561	orthogneiss	LHC	20	2.140	330	59.053	9108	10.599	5104	22	6.3	0.6	2.40	0.14	123	64
RT05-203	2440	31.11178	77.60581	orthogneiss	LHC	18	1.904	246	32.351	4179	10.531	5104	35	10.1	0.9	2.41	0.32	74	35

[a]See Figure 1 for location. Rho-D, induced track density in external detector adjacent to dosimetry glass ($\times 10^6$ tracks/cm^2); Nd number of tracks counted in determining Rho-D; Rho-S, spontaneous track density; Ns, number of spontaneous tracks counted; Rho-I, induced track density in external detector (muscovite); Ni, number of induced tracks counted; P, chi-square probability [*Green*, 1981; *Galbraith*, 1981]; Dpar, diameter of etched spontaneous fission tracks measured parallel to the crystallographic c-axis. Age, the sample pooled fission track age [*Hurford and Green*, 1983] calculated using zeta calibration method [*Galbraith and Laslett*, 1993]. Trackkey was used for calculating the counting results [*Dunkl*, 2002]. The following is a summary of key laboratory procedures. Samples were all analyzed by R. Thiede (zeta factor of 330 ± 21). Apatites were etched for 20 s in 5.5 M nitric acid at a temperature of 21.0 ± 0.1°C. CN5 dosimetry glass was used as a neutron flux monitor. Samples were irradiated at Oregon State University TRIGA reactor. External detectors were etched in 40% HF, 21°C, 45 min. Tracks were counted with a Leica microscope with 100× air objective, 1.25× tube factor, 10× eyepieces, using transmitted light with supplementary reflected light as needed; external detector prints were located with kinetic computer-automated scanning stage [*Dumitru*, 1993]. The AFT analysis employs the external detector method following the zeta calibration approach of *Hurford and Green* [1983]. Analytical precisions with and error low as 0.2 (±1 s) could be obtained from these young AFT ages because of the high U-content and the large number of grains counted per sample. Only grains with c axes parallel to slide plane were dated; zero-track grains were analyzed.

Valdiya, 1980]. Within the NW Himalaya, the HH is composed of both the HHC and LHC units and today highly elevated with peak elevations of ~7 km. Both HHC and LHC rocks have been thrusted over rocks related to the LH on a series of a series of ductile thrust systems named the Munsiari Thrust primarily during the early to middle Miocene [e.g., *Robinson et al.*, 2003]. The LH consists of Proterozoic to Palaeozoic (metasedimentary) sedimentary rocks with minor fractions of granites and gneisses and is bounded by the MBT to the south.

3. Methods: Thermochrononology, Thermal Modeling, Rainfall, and Specific Stream Power

[9] In regions that have experienced significant exhumation, thermochronometer cooling ages record the time since cooling below an effective closure temperature of specific minerals [*Dodson*, 1973]. If the distance from the closure-temperature isotherm to the surface can be estimated, then time-averaged exhumation rates can be provided for timescales of millions of years. Estimation of the closure-temperature depth is often achieved using 1-D, 2-D, or 3-D thermal models of different complexity [e.g., *Ehlers et al.*, 2005; *Reiners et al.*, 2005; *Whipp and Ehlers*, 2007; *Whipp et al.*, 2007]. We constrain the erosional-exhumation history of the NW Himalaya by using several geochronologic systems and a 1-D thermal model for the same region. A brief background to each of the methods used is given below.

3.1. Thermochronologic Analysis

[10] Twenty-four new AFT cooling ages were analyzed in this study using the external detector method [*Dumitru*, 2000; *Naeser*, 1979; *Wagner and Van den Haute*, 1992]. Further details on the approach are provided in Appendix B. All samples were obtained from bedrock exposed within HHC, LHC, and crystalline nappes covering LH sedimentary units between the Bhagirati River (upper Ganges) in the east and the Sutlej River in the west (Figures 1a and 1b). Additional sample preparation details are provided in Table 1. The young (<5 Ma) AFT cooling ages imply rapid transit through the partial annealing zone, which limits annealing. An effective closure temperature of 135 ± 10°C has been estimated for cooling rates between 70 and 100°C Ma^{-1}. All ages presented in this study pass the chi-square test, and central ages are reported with 1σ error. We interpret the AFT cooling ages as a proxy for the rate of exhumation.

[11] To obtain elevation-independent AFT-cooling ages for the exhumation rate calculation the samples were projected onto the average elevations of 1 and 3 km for LH and HH units, respectively. Elevation corrections were applied by using the slope of local age/elevation relationship (e.g., Figure 2). Because of to the lack of an age/elevation relationship of the TH AFT data, only LH and HH-cooling ages were corrected.

3.2. Thermal Modeling: Estimating Range of Exhumation Rates

[12] Thermal modeling is a well-established approach used to quantify time-averaged exhumation rates [e.g., *Ehlers and Farley*, 2003; *Laslett et al.*, 1987; *Mancktelow and Grasemann*, 1997; *Purdy and Jaeger*, 1976]. To evaluate the range of rates required to obtain observed AFT, ZFT and $^{40}Ar/^{39}Ar$-wM cooling ages, we used the AGE2EDOT program by *Brandon et al.* [1998; see also *Ehlers et al.*, 2005]. This program solves the steady state advection diffusion equation for user-defined initial conditions and material properties. Sample-cooling histories through the thermal field are tracked and cooling rate–dependent cooling ages are calculated using an effective closure temperature. A consequence for rapidly exhumed regions is that thermal advection dominates the thermal history over the influences of thermophysical properties and basal heat flux [*Mancktelow and Grasemann*, 1997; *Stüwe et al.*, 1994]. The assumption of a steady state thermal field is justified because of the short timescale required for the upper crust to reach thermal equilibrium in rapidly eroding regions [*Rahl et al.*, 2007; *Reiners and Brandon*, 2006]. For example, thermal steady state is 90% reached by ~1 Ma for AFT data if the exhumation rate is increasing >1 mm a^{-1}; Steady state is reached within ~5 Ma for $^{40}Ar/^{39}Ar$-wM data if the exhumation rate decreases from 2 to 3 mm a^{-1} to <1 mm a^{-1}. A more detailed justification for our use of a 1-D and steady state thermal model is given in Appendix B.

[13] In the model, the thermal field is represented by a steady state solution for a layer with thickness L, a thermal diffusivity κ, a uniform internal heat production rate H_T, a surface temperature, and an estimate of the initial near-surface thermal gradient for no exhumation. To obtain a range of exhumation rates we conducted a systematic survey of geologically possible values of κ, H_T, T_s, and G_T. More specifically, we varied κ, H_T, the near-surface thermal gradient and kept L and T_s constant. We determined the upper, intermediate, and lower limit for κ, H_T, and the mean thermal gradient for the upper 30 km (Table S2). For each of the thermochronometers we conducted at least 27 simulations surveying each combination of the input parameter. We identified the range of exhumation rates that could produce the observed cooling ages. We extracted four solutions for each thermochronometer, which cover the upper and lower limits of the thermophysical properties of rocks exposed in the Himalaya (see Figures S1, S2, and S3 within the supplementary material).[1]

[14] A limited number of studies provide constraints on the thermal physical properties of rocks exposed in the Himalaya [*England et al.*, 1992; *Ray et al.*, 2007; *Whipp et al.*, 2007]. The thermal parameters we used are presented in Table S2 in the supplementary material. In addition, we also considered six new thermal conductivity measurements from rocks in the study area. Results and further details are provided within the supplementary material and Table S2. On the basis of our own and previously published measurements we used thermal conductivity values ranging between ~3.5 and 2.0 W m^{-1} K^{-1} to calculate the thermal diffusivity [*Ray et al.*, 2007] (and own new data). HHC rocks are known to have a high U content causing high volumetric heat production with H_T values ranging between 3.0 and 0.8 μW m^{-3} [e.g., *England et al.*, 1992; *Roy and Rao*, 2000] as compared to the LHC and LH which are characterized by H_T values of ~0.8 μW m^{-3}.

[1] Auxiliary materials are available in the HTML. doi:10.1029/2008JF001010.

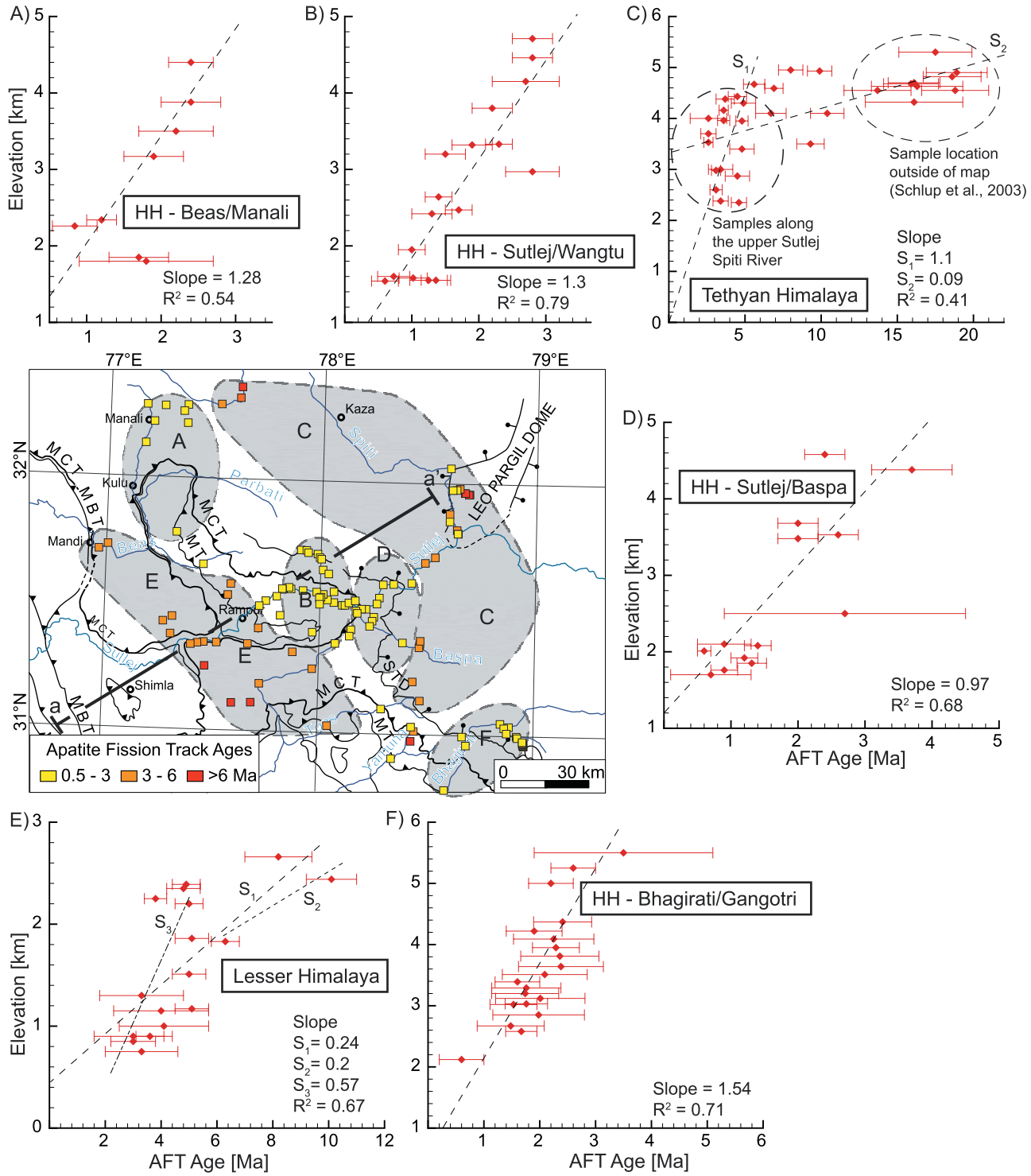

Figure 2. (a–f) AFT data divided into six regional groups and plotted against elevation. See map for location. Line a-a' shows the orientation of the cross section in Figure 3. TH, Tethyan Himalaya; HH, High Himalaya; LH, Lesser Himalaya.

[15] Peak metamorphic conditions in the HHC and LHC provide valuable constraints on model simulations. By late Oligocene–early Miocene (~23 Ma) the upper crust reached peak metamorphism conditions of 600–750°C at 8 kbar depth, leading to the formation of the HHC [e.g., *Dezes et al.*, 1999; *Searle et al.*, 1999; *Vannay and Grasemann*, 2001]. The LHC reached 600–700°C at 8 kbar depth by ~11 Ma [*Caddick et al.*, 2007; *Chambers et al.*, 2008; *Vannay et al.*, 2004]. Using these geologic constraints we assumed that basal temperature must be approximately around peak metamorphism temperatures and that the geothermal gradient was between 25 and 45°C km^{-1} from the early Miocene onward. A model depth of L ~30 km roughly matches the depth of the basal

décollement of the Main Himalayan Thrust and the maximum burial during peak metamorphism, respectively. We used these petrologic data to provide a lower constraint for estimated exhumation rates, and explored the sensitivity of our results to different depths and temperatures of the basal boundary condition. We found that differences in predicted ages were within sample uncertainties and the results presented here are relatively insensitive to the assumed basal condition because of the high exhumation rates of the region, as found by *Whipp et al.* [2007].

3.3. Relief Analysis

[16] Early assessments of landscape-scale exhumation rates resulted in a linear relation between exhumation rate and mean local relief for midlatitude drainage basins [*Ahnert*, 1970]. Subsequently, *Summerfield and Hulton* [1994] concluded from a global study that local relief and runoff are the dominant controls on exhumation rate for major drainages. Ahnert's linear correlation does not hold for data from tectonically active areas, for which *Montgomery and Brandon* [2002] suggested a power law function relationship between exhumation rate and relief. If so, is there a relationship between relief and megaannum timescale exhumation rates in the NW Himalaya? For the relief analysis we used processed Shuttle Radar Topography Model 90 m digital elevation models (DEM) V. 3.0 A. Jarvis, unpublished data, 2004 (available at http://srtm.csi.cgiar.org and http://www.ambiotek.com/topoview) and calculated the local relief by measuring the difference between minimum and maximum elevation within 2.5, 5, and 10 km diameter windows around each pixel in the DEM.

3.4. Rainfall Measurements

[17] In mountainous regions the distribution of orographic rainfall is highly variable. For the Himalayan front recent work has estimated rainfall amounts from satellite data using the Tropical Rainfall Measurement Mission (TRMM) [*Bookhagen and Burbank*, 2006]. The TRMM satellite provides daily rainfall estimates on a $\sim 5 \times 5$ km pixel size and was calibrated with ground-based rainfall measurements from Central Nepal and Bhutan [*Barros et al.*, 2000; *Bookhagen and Burbank*, 2006; B. Bookhagen and D. W. Burbank, Controlling factors for monsoonal rainfall distribution and its implication for specific stream power amounts in the Himalaya, submitted to *Journal of Geophysical Research*, 2008]. The data have been processed for a 9 year period (1998–2006) and mean annual rainfall amounts have been integrated over the watershed to produce river discharge assuming 100% surface runoff and no storage for the specific stream power analysis. We calculated annually averaged accumulated flow amounts using the 90 m flow-routing grid derived from the patched topographic data. Further details of data processing are described by *Bookhagen and Burbank* [2006; also submitted manuscript, 2008].

3.5. Specific Stream Power

[18] The regional distribution of specific stream power (SSP) across the study area was calculated to quantify a proxy of modern erosion potential. Our SSP model is a proxy for fluvial erosion based on channel slope, channel width, and river discharge. Total stream power per unit channel length Ω (W m^{-1}) is calculated by multiplying the specific weight of water γ ($\gamma = \rho_w g = 9810$ N m^{-3}), where ρ_w is the density of water and g denotes gravity acceleration) with the water discharge Q(m^3 s^{-1}) and energy slope S (m m^{-1}), which may be approximated by the slope of the channel bed [*Bagnold*, 1966, 1977; *Knighton*, 1998]. The total stream power is an expression for the rate of potential energy expenditure per unit length of channel.

[19] The corresponding specific stream power ω (W m^{-2} or J m^{-2} a^{-1}) is given by Ω divided by the channel width w (m) or by multiplying the mean boundary shear stress τ_0 (N m^{-2}) and the mean flow velocity v (m s^{-1}). This equation defines the rate at which potential energy is supplied to a unit area of the bed. Stream power is influenced by the integrated effects of channel slope, discharge, and channel width, of which the latter two parameters are difficult to derive. Usually, discharge is derived as a power law function of area, and channel width is assumed to scales with discharge. The catchments in the Himalaya exhibit a very steep rainfall gradient caused by orogeny along the HH resulting in a steep discharge gradient that is in turn difficult to capture in a power law relation. Here, we use calibrated TRMM values that predict discharge for the Himalayan catchments. Bedrock channel width usually exhibits a power law relation with discharge ($w = Q^b$). Valid values for b in bedrock channels have been suggested to be between 0.3 to 0.5 [*Leopold and Maddock*, 1953; *Montgomery and Gran*, 2001]. We use an exponent of 0.4. This value has been found to be a valid scaling factor in mountainous catchments in the Marsyandi River of central Nepal [*Craddock et al.*, 2007]. We calculated specific stream power amounts for every point in the landscape and applied a 10 km smoothing filter to remove any local effects, but maintain the general pattern and produce a coherent SSP map.

4. Results

[20] In the following section, we introduce the new AFT ages and put them in regional perspective with published data. Next, we analyze the entire data set by looking at age–elevation relationships and regional changes, and provide preliminary characteristics for exhumation. Subsequently we determine averaged exhumation rates as a function of AFT, ZFT, and ^{40}Ar/^{39}Ar-wM cooling ages by applying thermal models. The average exhumation is converted into transient exhumation rates for certain time intervals. Finally, we correlate the exhumation rates with topographic relief, rainfall, and specific stream power, to characterize spatiotemporal variation of exhumation across the southern Himalayan front.

4.1. New Apatite Fission Track Data

[21] Twenty-four new AFT samples yield cooling ages between 10.8 ± 1.8 and 0.6 ± 0.2 Ma (1σ error). Analytical results are shown in Table 1 and Figure 1. In general, the samples mostly characterized by moderate U content provide robust AFT ages (five representative radial plots are presented in Figures 3a, 3b, 3c, 3d, and 3e). The ages can be subdivided into three groups with respect to their age, elevation, and tectonomorphic regions (LH, HH, TH):

[22] 1. Within the LH, 8 samples yield ages between 10.1 ± 0.9 and 3.0 ± 0.4 Ma for sample elevations between

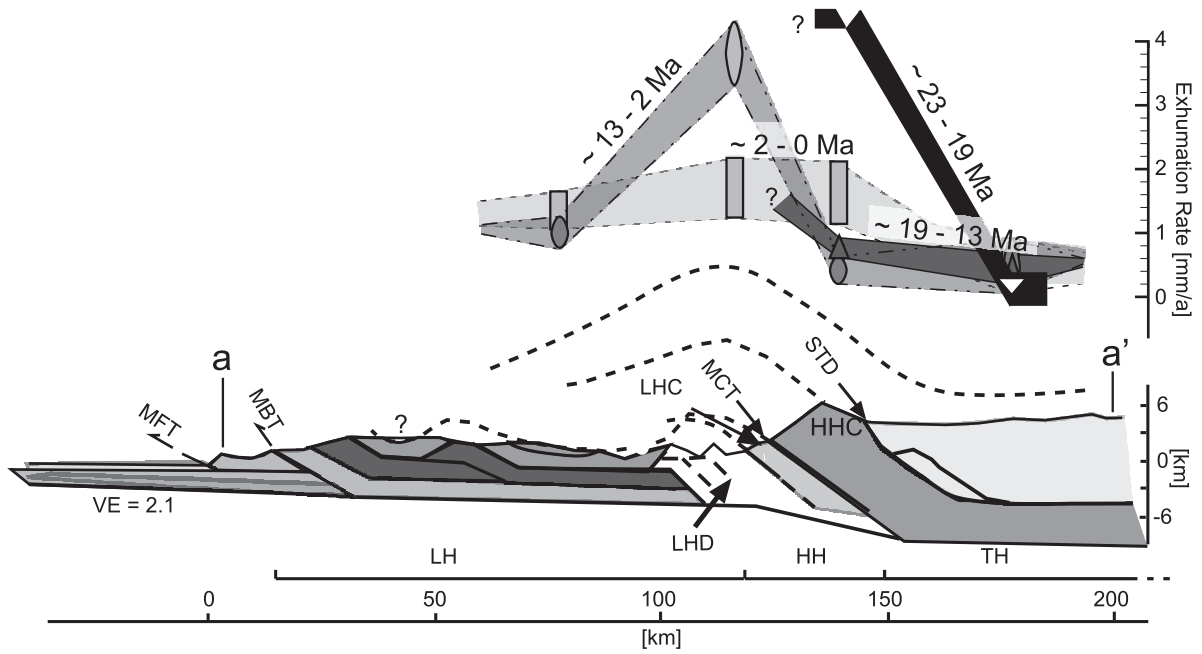

Figure 3. Temporal and spatial variations in exhumation across the NW Himalaya related to a schematic cross sections derived from previous studies [*Robinson et al.*, 2006; *Srivastava and Mitra*, 1994; *Vannay et al.*, 2004]. See Figure 2 for the location of the cross section. Regional distribution of exhumation rates was determined from the 1-D thermal model (see section 4.3 for further details). Dashed lines in the cross section indicate estimates of volume loss due to erosion since the early Miocene. HHC, High Himalayan Crystalline; LHC, Lesser Himalayan Crystalline; LHD, Lesser Himalayan Duplex; MCT, Main Central Thrust; STD, Southern Tibetan Detachment; MBT, Main Boundary Thrust; MFT, Main Frontal Thrust.

800 and 2700 m a.s.l. (shown as diamonds in Figure 1b). These ages suggest minimum cooling rates between ~12° to 45°C Ma^{-1} for transit between an estimated closure temperature of 125 ± 10°C and the surface (Figure 4). All samples were of granitic or metamorphic origins that form nappes covering sedimentary units in the Lesser Himalaya. For the LH the obtained ages are strongly elevation-dependent (Figure 2e), with ages of 10 to 8 Ma for elevations >2000 m a.s.l. The majority of the AFT samples obtained at moderate elevations (<2000 – 500 m) yield cooling ages between 6 and 3.5 Ma.

[23] 2. Along the southern front of the HH, the 14 AFT ages are generally younger than those in the LH, ranging from 3.6 ± 0.5 to 0.6 ± 0.2 Ma, and are consistent with earlier studies [*Sorkhabi et al.*, 1996; *Thiede et al.*, 2004; *Vannay et al.*, 2004]. Sample elevations ranged between 1200 and 5000 m a.s.l. (squares in Figure 1b), and suggest cooling rates between >200° and ~40°C Ma^{-1}. The only exception we obtained is the age of sample RT05–108

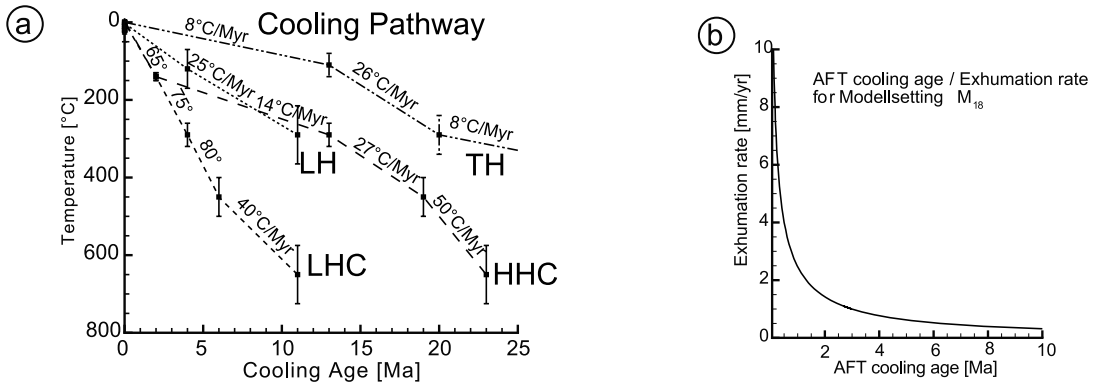

Figure 4. Representative regional mean cooling histories and example of model result for converting AFT ages to exhumation rates. (a) Cooling pathway of the tectono-morphic provinces constrained by closure temperatures of the corresponding thermochronometer and peak metamorphism conditions. Abbreviations are the same as in Figure 3. (b) Relationship between AFT cooling age and exhumation rate for K = 3.6 W m^{-1} K^{-1}. Ht = 3.1 W 10^{-6} m^{-3} of model M_{18}. Note that a small change in thermochronometer age corresponds to a large variation in exhumation rates for AFT ages <1–2 Ma.

Table 2. Results: Modeled Exhumation Rates[a]

Unit	Total Number of Samples	Elev.-d	Age (Ma)			Figure	Exhumation Rates (mm a^{-1})						
			Range	Mean	SD		Minimum	Maximum	Mean	SD	W-Mean	Duration (Ma)	Corrected	$\Delta t = tx - ty$ (Ma)
TH_{AFT}	(48)	40(4 ± 1 km)	1.9–39.9	12.3	9.17	S1b and S1d	0.1	1.8	0.51	0.38		13	0.5 ± 0.4	13–0
TH_{ZFT}	29		13.6–45.0[b]	30.7	11.2	S2b and S2d	0.3	0.8	0.31	0.14		7	0.4(E2) ± 0.1	20–13
$TH_{Ar/Ar}$	9		32.6–53.8[c]	29.8	16.3	S3b and S3d	0.4	1.2	0.30	0.32		20	0.2(E3) ± 0.3	40–20
HHC_{AFT} = (HHC + LHC)	(79)	45(3 ± 1 km)	0.6–3.6	1.86	0.65	S1b and S1a	0.9	3.7	1.52	0.54	1.54	2	1.5 ± 0.5	2.0–0
HHC_{ZFT}	11		6.1–19.9	13.4	3.6	S2b and S2a	0.5	0.8	0.55	0.14		11	0.4(E2)± 0.1	13–2
$HHC_{Ar/Ar}$	38		9.7–22.3	18.5	2.8	S3b and S3a	0.4	0.8	0.63	0.11		6	0.8(E3) ± 0.1	19–13
HHCpeak meta (~8 kbar = 30 km depth)[d]			23.0						1.30			4	4.5(E4) ± 0.2	23–19
LHC_{AFT} = (HHC + LHC)	(79(HHC + LHC))	45(3 ± 1 km)	0.6–3.6	1.86	0.65	S1b and S1c	0.9	4.3	1.52	0.54	1.54	2	1.5 ± 0.5	2.0–0
LHC_{ZFT}	8		1.4–4.8	2.3	1.1	S2b and S2c	1	3	2.40	0.65		2	3.2(E2) ± 0.7	4.0–2
$LHC_{Ar/Ar}$	14		4.4–14.9	6.2	2.7	S3b and S3c	1.8	2.9	1.75	0.40		2	2.0(E3) ± 0.4	6–4.0
LHCpeak meta (~8 kbar = 30 km depth)[d]			11.0						2.73			5	3.9(E4) ± 0.5	11–6.0
LH_{AFT}	(19)	13(1 ± 1 km)	2.5–6.3	4.16	1.08	S1d and S1cc	1.3	2.4	1.61	0.38	1.41	4	1.4 ± 04	4.0–0
LH_{ZFT}	10		9.6–12.2	10.9	1.3	S2d and S2c	0.8	2.5	1.17	0.10		7	1(E2) ± 0.1	11–4.0

[a]Unit, morphotectonic unit; Elev.-d, number of samples within an elevation envelope (shown in parentheses); Range, of obtain cooling age population; Mean, arithmetic mean; W-Mean, weighted mean; E2 = [(E0t0) − (E1t1)](t0 − t1); E3 = [(E0t0) − (E1t1) − (E2t2)](t0 − t1 − t2)$^{-1}$; TH, Tethyan Himalaya; HHC, High Himalayan Crystalline; LHC, Lesser Himalayan Crystalline; LH, Lesser Himalaya.
[b]Sample with age >50 Ma ignored.
[c]Sample with age <20 Ma and >60 ignored.
[d]Data from *Vannay et al.* [2004] and *Caddick et al.* [2007].

(10.8 ± 1.8 Ma), which was unexpectedly old compared to neighboring samples to the north (3.6 ± 1.8 Ma) and south (2.0 ± 0.4 Ma).

[24] 3. Cooling ages from the hanging wall of the STDS range between 3.4 ± 0.5 and 4.5 ± 0.6 Ma at elevations between 2300 and 4500 m a.s.l., and suggest cooling rates of ~30° to 40°C Ma^{-1} (triangles in Figure 1b).

4.2. Regional Variations in Thermochronometer Age/Elevation Relationships

[25] To evaluate spatial variations in the AFT data (new and published) we divided the data into six regional groups (Figure 2). The high data density along the southern margin of the HH allowed us to divide this region into four subgroups (Figures 2a, 2b, 2c, and 2f), whereas TH (Figure 2c) and LH (Figure 2e) data are compiled into a single group. All HH sample groups yield consistently young ages (<3 Ma). Nonetheless, a clear age/elevation relationship exists. The range of slopes of error-weighted regression lines through sample ages versus elevation yield slopes and average R^2 correlations of 1.0 to 1.5 mm a^{-1} and 0.68, respectively. We note much less variability in the slopes compared to transects in central Nepal [*Blythe et al.*, 2007], suggesting that the entire High Himalaya has been subjected to rapid exhumation for at least the last 3–4 Ma, if not longer. In contrast, the TH and LH sample groups are characterized by older, and more variable AFT ages (Figures 3c and 3e), suggesting slower cooling rates. Moreover, the TH data suggest that the TH has stayed within the upper 3 km of the crust for >5 Ma or even 30 Ma, except regions near recently exhumed domes, such as the Leo Pargil dome, or deeply incised river valleys, such as the upper Sutlej Valley [e.g., *Thiede et al.*, 2006].

[26] Age/elevation relationship can provide information on temporal variations in exhumation. However, none of the slopes obtained by the regression of the AFT age/elevation relationship in this study can be rigorously related to true exhumation rates because the combination of the large lateral distances over which transects were collected, and high-relief and long-wavelength topography likely invalidate the assumptions required to quantify rates using the slope of regression lines [*Braun*, 2002; *Stüwe et al.*, 1994]. In summary, the observed age-elevation relationship is not only the result of vertical exhumation, but also potential changes in relief, oblique exhumation and/or spatial variations in exhumation, and topography.

4.3. Numerical Modeling and Transient Exhumation Rates

[27] By conducting 75 1-D thermal model simulations we explored the range of possible exhumation rates as a function of AFT, ZFT and $^{40}Ar/^{39}Ar$-wM cooling ages (results summarized in Table 2 and in Figures S1, S2, and S3 in the supplementary material). We identified exhumation rates that vary in space and time between 0.1 and 4.5 mm a^{-1} across the Himalaya between the Miocene and Present. This range was identified by using our best estimate for thermophysical properties and boundary conditions of the different tectonomorphic provinces (Table S2, within the supplementary material). We note that recent work by *Whipp and Ehlers* [2007] highlights the significance of fluid flow in biasing exhumation rate calculations in the Nepalese Hima-

laya. A full consideration of the effect of fluid flow on our calculated exhumation rates is beyond the scope of this study because of the size of the data set analyzed and large geographic region considered. However, we emphasize that if fluid flow does significantly influence the thermal field in the study area then our calculated exhumation rates should be regarded as minimum estimates of the true exhumation rate [cf. *Whipp and Ehlers*, 2007]. We discuss this in additional detail in section 5.1.

[28] Our exhumation rates yield a time-averaged rate. While useful, this approach fails to account for changes in exhumation that postdate passage through each minerals closure temperature. Transients in the exhumation history of the samples can be more accurately quantified if, for example, the time-averaged ZFT derived rate is corrected for any change in the rates recorded by the AFT sample. Rather than reporting the time-averaged rates from sample closure to the Present we follow the approach of *Ehlers et al.* [2003] and report the exhumation rates between closure of the individual systems in Table 2 (e.g., between 13 and 2 Ma, and 2–0 Ma in our following example). To a first approximation, this approach is justified because in rapidly eroding regions the near surface thermal field rapidly achieves a new steady state (1–5 Ma) in response to changing exhumation rates (see also Appendix A).

[29] Our method for calculating the transient exhumation rates for each thermochronometer system is as follows. Consider a suite of AFT and ZFT ages used to determine exhumation rates of HHC rocks for the last 13 Ma. Mean ZFT ages (13.4 ± 3.6 Ma) suggest an average exhumation rate of 0.55 mm a^{-1} (E_0) for the last ~13 Ma (t_0) (HHC_{ZFT} (Table 2)), while mean AFT ages (1.9 ± 0.7 Ma) represent an average exhumation rate (E_1) of ~1.52 mm a^{-1} (HHC_{AFT} (Table 2)) for the last 1.9 ± 0.7 Ma (t_1). Thus, the exhumation rate (E_2) for the period between 13 and 2 Ma must have been lower and is given by

$$E_2 = [(E_0 t_0) - (E_1 t_1)](t_0 - t_1)^{-1}. \quad (1)$$

[30] Applying the previous values for (E_0), (E_1), (t_0), and (t_1) in equation (1) suggests an exhumation rate of 0.4 mm a^{-1} between ~13 and 2 Ma and that exhumation has increased by a factor of ~3–4 (from 0.4 to 1.52 mm a^{-1}) since ~2 Ma. A similar approach was used to obtain the exhumation rate (E_3) as a function of the $^{40}Ar/^{39}Ar$ sample ages between 19 and 13 Ma. In this approach the HHC has been eroded at an average rate (E_0) of 0.63 mm a^{-1} for the last (t_0) ~19 Ma ($HHC_{Ar/Ar}$ (Table 2)) and the ZFT and AFT has been eroded at average rates of (E_2) of 0.4 mm a^{-1} for (t_2) ~13–2 Ma and (E_1) ~1.5 mm a^{-1} for (t_1) of ~2 Ma. Therefore, the exhumation rate (E_3) for the period between 19 and 13 Ma must have been higher and is given by

$$E_3 = [(E_0 t_0) - (E_2 t_2) - (E_1 t_1)](t_0 - t_2 - t_1)^{-1}. \quad (2)$$

[31] This suggests an exhumation rate of 0.8 mm a^{-1} between ~19 and 13 Ma, which then decreased by a factor of 2 from 13 Ma onward.

[32] Finally, we can also determine exhumation rates between the interval from the onset of decompression subsequent to peak metamorphism at ~23 Ma for HHC and ~11 Ma for the LHC, and the $^{40}Ar/^{39}Ar$ cooling ages. Both units were at a depth of ~30 km (~8 kbar) during peak metamorphism. Using the same approach as above, we can determine the exhumation rate (E_4) for the HHC for the period between 23 and 19 Ma ($HHC_{peak\text{-}meta}$ (Table 2)) given by

$$E_4 = [(E_0 t_0) - (E_3 t_3) - (E_2 t_2) - (E_1 t_1)](t_0 - t_3 - t_2 - t_1)^{-1}. \quad (3)$$

[33] This suggests high exhumation rates of 4.5 mm a^{-1} immediately after peak metamorphism, followed by a decrease of a factor of ~6 at ~19 Ma. The same approach has also been applied to the LH, LHC, and TH and the results are presented in Table 2 and Figure 3.

4.4. Relief

[34] Calculation of local relief over radii of 2.5, 5 and 10 km produced no discernable difference in the pattern of relief change over the study area (Table S2 in the auxiliary material). For brevity, in the following we only present relief averaged over 5 km distance. Figure 5a illustrates the regional distribution of the local relief and the range of cooling ages for reference (see Figure 5c for legend on ages). The three tectono-metamorphic groups LH, HH, and TH show characteristic differences in the spatial distribution of relief. For example, the mean relief at the AFT sample locations is highest in the HH and averages ~2.55 km (i.e., compare yellow squares with blue shaded regions). Relief is lower in both the TH and LH with averages of ~1.93 and 1.65 km, respectively. We found little to no correlation between AFT cooling ages and relief. Similarly poor correlations were found when comparing cooling ages to local slope (results not shown). Also, no clear correlation, however, were observed between modern relief and higher-temperature thermochronometer systems (e.g., ZFT, Ar-wM) was found (Figures 6a, 6b, and 6c).

4.5. Rainfall

[35] Rainfall has a first-order control on discharge, and therefore directly affects fluvial erosion. In the NW Himalaya rainfall maxima of >2 m a^{-1} are located SW of the HH, south of the highest relief and topography, for details see *Bookhagen and Burbank* [2006]. The magnitude of precipitation decreases dramatically to <0.5 mm a^{-1} along the boundary between HH and TH (Figure 5b). This is due to the high elevated HH functioning as an orographic barrier to rainfall.

[36] In general, we find a poor correlation between megaannum timescale exhumation rates and mean annual rainfall (Figures 6c and 6d). Similar observation have been made in central Nepal [*Burbank et al.*, 2003]. A more detailed comparison between exhumation rates and rainfall is not warranted because the magnitude of fluvial erosion near each sample location depends heavily on the integrated rainfall rate upstream from the sample location, not just the amount of rainfall near the sample location. Thus, as presented next, comparisons between exhumation rates and specific stream power should be more meaningful.

4.6. Specific Stream Power

[37] Results from our SSP analysis indicate stream power ranges between <5 and >100 W m^{-2}. As shown in Figure 5c

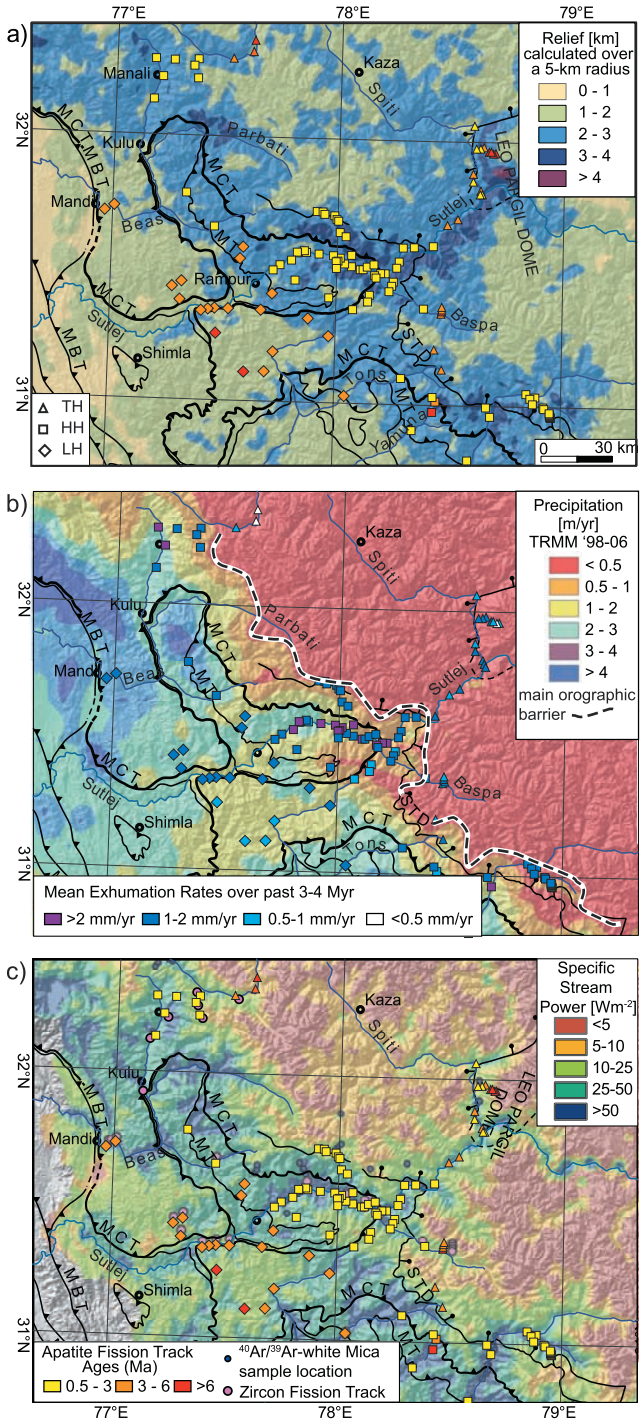

Figure 5. Spatial relationship between AFT cooling ages and (a) relief, (b) present-day mean annual rainfall and exhumation rates, and (c) specific stream power (SSP).

the higher values are located in steep and deeply incised valleys within the HH. In general, SSP values within the HH are two to four times higher than in the LH and TH, respectively. Regions with the highest SSP typically correspond to places with high mean annual precipitation and relief (e.g., compare Figure 5c with Figures 5a and 5b).

[38] The comparison of exhumation rates with specific stream power resulted in slightly improved correlations (Figures 6e and 6f) compared to correlations with rainfall because the upstream contributing area of rainfall at a sample location is accounted for. Over timescales >5 Ma (Figure 6e), a high correlation (R^2 = 0.61) between exhumation rates derived from wM-Ar samples and specific stream power was limited to the TH. For all other regions we obtain poor correlations (R^2 < 0.21). Over timescales <3 Ma (Figure 6f), only the TH show a moderately positive correlation (R^2 = 0.63) with AFT-derived exhumation rates.

5. Discussion

[39] In the following we discuss how exhumation rates varied over different time intervals from the early Miocene to recent. Subsequently, we evaluate why poor correlations are found between long-term exhumation rates and present-day topographic relief, rainfall, and specific stream power. We conclude on the basis of our analysis of the spatial variations in exhumation across the NW Himalayan front that both climate and tectonics are drivers for the observed exhumation patterns.

5.1. Spatial and Temporal Variations in Exhumation

[40] Exhumation rates calculated in this study suggest that the three main tectono-morphic units are characterized by large spatial and temporal variations in exhumation (Table 2) and cooling rate (Figure 4a). A synthesis of the exhumation history is calculated over different time intervals using equations (1)–(3) and is presented in Figure 3 as follows:

[41] 1. Between ~23–19 Ma, following peak metamorphism of the HHC, our results suggest exhumation rates >3 mm a^{-1}.

[42] 2. Between ~19–13 Ma exhumation rates decreased by a factor of ~6, and were between ~0.5 and 0.7 mm a^{-1}.

[43] 3. Between ~13–4 Ma exhumation rates remained low (~0.5 mm a^{-1}) in the HHC, but increased to ~3 mm a^{-1} within the LHC. Within the LH exhumation rates are low and ~0.8 mm a^{-1} since 10 Ma.

[44] 4. Finally, exhumation rates over the last 3 Ma increase to ~1–2 mm a^{-1} within the LHC and HHC, and decrease <1 mm a^{-1} both in the TH to the north and the LH to the south. In summary, the highest exhumation rates (~3–4 mm a^{-1}) documented in this part of the Himalaya occurred between ~23–19 Ma, followed by a pulse of rapid exhumation (~3 mm a^{-1}) between ~13–2 Ma farther south in the LHC. This later pulse of exhumation in the LHC is possibly the result of emplacement and exhumation of crystalline nappes of the HHC and LHC on top of the LH. In addition it may result from continuous development of the Lesser Himalayan Duplex [*DeCelles et al.*, 2001].

[45] Finally, we observe relatively uniform and broadly distributed exhumation between 3 and 0 Ma across the LHC and HHC (step 4 above), which does not show any variability across individual structures. Two possible explanations for this include that (1) variations in exhumation rate across active structures during this time are not discernible, as *Whipp et al.* [2007] suggested; alternatively, (2) broadly distributed exhumation at this time could indicate climatic (because of repeated perturbation or continuous oscillation on short timescales persisting on million year timescales), rather than tectonic forcing.

[46] For the interpretation of exhumation rates and to measure pronounced changes in erosion, it is important to note that the sensitivity of thermochronometer-cooling ages to identify variations in exhumation decreases significantly when exhumation rates are high (>2 mm a^{-1} (Figure 4b)), see also [*Rahl et al.*, 2007]. The poor sensitivity is a function of thermal diffusivity, and the compression of isotherms underneath topography with rapid exhumation.

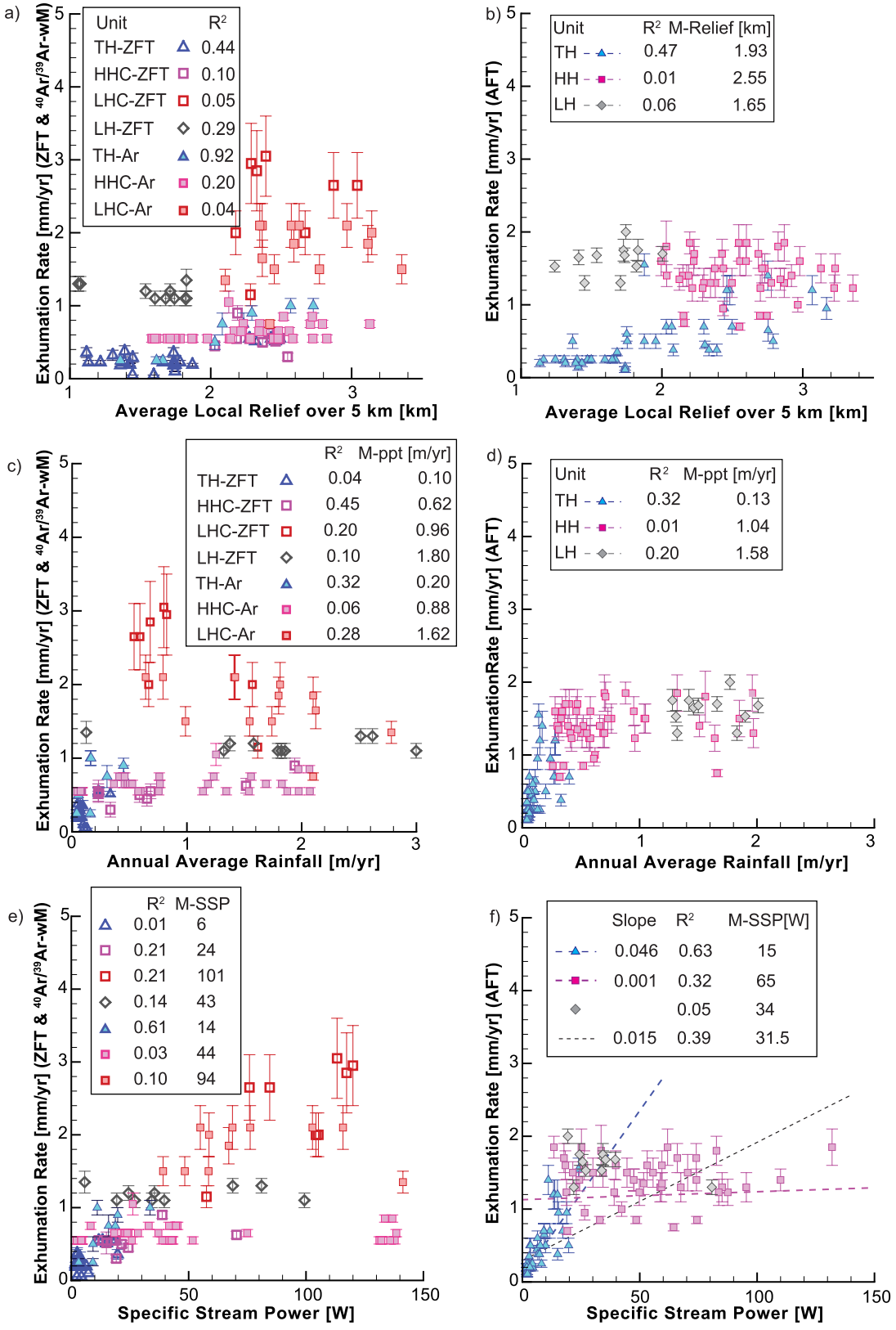

Figure 6

This is illustrated in the model result shown in Figure 4b, where, for example, for very young AFT cooling ages (<1 Ma) small changes in age cause large changes in exhumation rate, and model uncertainties, during rapid exhumation (~2 to 5 mm a^{-1}) can exceed 1 mm a^{-1}. In contrast, at low exhumation rates (<0.5 mm a^{-1}) the errors can be low as 0.2 mm a^{-1}. This inherent limitation to interpreting variations in exhumation rates in rapidly denudating regions is often overlooked by other studies in the Himalaya [e.g., *Burbank et al.*, 2003]. Given this limitation, exhumation rates of >1–2 mm a^{-1} from AFT data should therefore be thought of as minimum estimates of the rate, and the true rate could be significantly higher by a factor of 2 or 3. Despite these uncertainties, significant temporal variations in the exhumation rate were obtained across the Himalayan front. For example, exhumation rates in the LHC and HHC units vary by greater than a factor of 4, depending on the time interval analyzed. The implications of these variations are discussed below.

[47] One caveat to our calculation of exhumation rates is that we do not account for the impact of upper crustal fluid flow on cooling ages. *Whipp and Ehlers* [2007] suggest that fluid flow influences cooling ages and thermochronometer derived exhumation rates in the Himalaya. The approach used here does not account for this effect because of the structural complexity of the region and large geographic region and number of samples considered. Rather, we note that (1) if fluid flow is significant in the region, then it is pervasive because age/elevation relationships in the HH are similar in terms of the slopes throughout the region, and (2) furthermore, if fluid flow is significant here, then the exhumation rates presented in our study are minimum estimates for each thermochronometer system, with the greatest impact being on the lower-temperature systems such as AFT [e.g., *Whipp and Ehlers*, 2007].

5.2. Exhumation Rate Versus Relief, Rainfall, and Specific Stream Power

[48] Here, we evaluate how well exhumation rates derived from thermochronometer data are correlated with the present-day climatic, geomorphic, and tectonic setting along the NW Himalayan margin.

[49] In general, we observe only a poor correlation between AFT-derived exhumation rates and relief, rainfall and SSP. In Figures 6b, 6d, and 6f the AFT-derived exhumation rates plot in discrete areas and only partially overlap. However, both rainfall and stream power plots (Figures 6d and 6f) show the same characteristics at the transition between TH and HH, suggesting that rainfall is the limiting factor. ZFT and $^{40}Ar/^{39}Ar$ data show a poor correlation, suggesting that the processes that controlled their exhumation are not related to the pattern of present-day relief, rainfall or SSP observed today.

[50] The poor correlations between exhumation rates versus relief, precipitation, and stream power (Figure 6) can be explained in several ways. One explanation is that both modern topography and erosion are not representative of conditions in the past at the time samples cooled. The topography, for instance, could be transient or decoupled from variations in rainfall over the last several million years. This is the case for the HH and LH, where we know that erosion was highly variable in space and time [*Bernet et al.*, 2006; *Bookhagen et al.*, 2005; *Burbank et al.*, 2003; *Clift et al.*, 2008; *Pratt et al.*, 2002]. However, the stronger correlation between relief and stream power with exhumation rates in the TH suggests that at least in this region exhumation may have occurred under topographic conditions with a similar relief as today. Second, as discussed above, the sensitivity of thermochronometer data to changes in exhumation rates is nonlinear and the sensitivity decreases at rates >~2 mm a^{-1} (e.g., Figure 4b). Interestingly, all plots in Figure 6 demonstrate an asymptotic behavior for erosion rates >1 mm a^{-1} by increasing young ages, while at rates <1 mm a^{-1}, which are typical for the TH, the behavior is more linear. Thus, the poor correlation between exhumation rates and the various morphometric parameters shown in Figure 6 are likely the result of a decreased sensitivity of thermochronometer data to changes in erosion in these regions characterized by high exhumation rates. Third, it is also possible that a strong correlation between long-term exhumation rates and relief or stream power could exist in our study area, but is not resolvable within uncertainties in the thermochronometer data.

5.3. Belt of Rapid Exhumation

[51] Figures 7 and 1a show strong variations in exhumation over an area of 200 × 150 km from AFT cooling ages that coincide with tectonomorphic units of the Himalayan front. More specifically, we identified a 30–40 km wide belt of rapid exhumation shown in Figure 7. This zone is characterized by cooling ages that are <3, ~4, ~6 Ma for AFT, ZFT, ArAr-wM, respectively, with calculated exhumation rates of ~3 mm a^{-1} between 11 and 2 Ma, before rates decrease to ~2 mm a^{-1}.

[52] The lateral extent of this zone (Figure 7) is significantly larger than previously thought [*Thiede et al.*, 2005], and is not as well correlated with the TRMM-derived rainfall data as was previously suggested. The belt of rapid exhumation extends parallel to the range front and its across-strike width of the belt and AFT cooling ages are generally invariant with respect to the present-day geometry of the MCT or MT thrusts within the NW Himalaya (Figure 7). The southern boundary of this zone coincides with a well-

Figure 6. Comparison between model-predicted denudation rate and the corresponding (a, b) relief, (c, d) rainfall, and (e, f) specific stream power (SSP) at each sample location. Figures 6a, 6c, and 6e are for the ZFT and $^{40}Ar/^{39}Ar$ thermochronometer systems, and Figures 6b, 6d, and 6f are for the AFT system. Local relief in Figures 6a and 6b was calculated over a 5 km radius circle using Shuttle Radar Topography Model 90m digital elevation model V. 3.0. The data in Figures 6a, 6b, 6c, 6d, 6e, and 6f are grouped according to the tectono-morphic units. R2, correlation coefficient; M-ppt, mean precipitation at the sample location; M-SSP, mean specific stream power; TH, Tethyan Himalaya; LH, Lesser Himalaya; HH, High Himalaya; AD, all data; TH-Ar, Tethyan Himalaya $^{40}Ar/^{39}Ar$-wM.

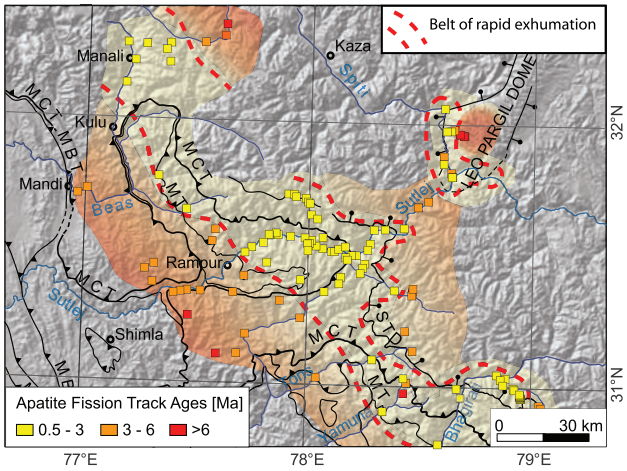

Figure 7. Belt of rapid exhumation defined by young AFT cooling ages along the southern Himalayan Front over the last 3 Ma. The width alongstrike varies, and AFT cooling ages are generally invariant with respect to the geometry of the MCT or MT thrusts within the NW Himalaya. The southern boundary of the area of high exhumation coincides with a well-defined break in slope near the LH-HH boundary. The northern boundary is not as clearly defined as the southern one and is characterized by a large embayment that extends ~20–40 km into the plateau. Such embayments coincide with major, deeply incised river valleys, such as the Sutlej or the Bhagirathi that drain the Tethyan Himalaya. The rapid exhuming region is bounded both to the north and south by sectors of moderate to slow exhumation (<2 mm a^{-1}). The lateral extent of this zone is significantly larger than previously suggested by *Thiede et al.* [2005] and runs parallel to the range front.

defined break in topographic height near the LH-HH boundary. These observations are consistent with recent studies in central Nepal that argue for a reactivation of the MCT [*Hodges et al.*, 2004; *Wobus et al.*, 2005, 2003]. However, the northern boundary is not as clearly defined as the southern one, and it is characterized by large embayments that extend ~20–40 km into the Tibetan Plateau. These embayments coincide with major and deeply incised river valleys, such as the Sutlej or the Bhagirathi that drain the TH. Finally, the rapidly exhuming region is bounded to the north and south by moderate to slow denuding regions, not exceeding rates of 2 mm a^{-1}. In summary the southern Himalayan front is characterized by a focused zone of exhumation, similar in magnitude to what is observed within the Himalayan syntaxes and in central Nepal [*Blythe et al.*, 2007; *Burg et al.*, 1998; *Whipp et al.*, 2007; *Zeitler et al.*, 2001].

[53] Over the last decade the channel flow models have emerged as a favored explanation for the high strain and high-grade metamorphism in the HHC [e.g., *Grujic et al.*, 1996; *Law et al.*, 2006; *Nelson et al.*, 1996]. The channel flow hypothesis suggests that ductile extrusion of High Himalayan Sequence might be linked through erosion along the southern edge of the plateau [*Beaumont et al.*, 2001; *Hodges et al.*, 2001; *Jamieson et al.*, 2006]. The data presented in this paper provide two constraints for future geodynamic simulations that test the channel flow hypothesis:

[54] 1. Observed spatial and temporal variations in erosional exhumation suggest two major changes of deformation caused by orogen internal reorganization and/or major climatic fluctuations since the early Miocene. The cause of these changes is unknown, although no clear tectonic mechanism has been identified so far.

[55] 2. Crystalline clippes covering parts of the LH imply that erosion has not been pervasive enough to balance extrusion and overthrusting of major High Himalayan crystalline nappes during the early and middle Miocene.

5.4. Exhumation of the Lesser Himalaya

[56] Apatite-poor, LH lithologies across much of the Himalayan front have hampered previous AFT studies from quantifying the long-term exhumation history. The NW Himalaya, however, has the advantage that remnants of crystalline nappes covering the LH have survived erosion and provide apatite-rich lithologies. Our new AFT data provide insights into the tectonic evolution of the Lesser Himalaya. These include (1) the 10 to 8 Ma AFT cooling ages obtained from high-elevation samples of the crystalline nappes, combined with earlier published 12 to 10 Ma ZFT cooling ages that suggest thrust sheet emplacement onto the LH was completed prior to ~10 Ma and (2) the majority of the AFT samples obtained at moderate and low elevations within the LH yield cooling ages between 6 and 3.5 Ma (Figure 2e), suggesting that rock uplift, river incision, and exhumation have been active since that time. Viewed in the context of the general tectonic evolution of the southern Himalayan front, our cooling age data indicate that the deformation and rapid rock uplift propagated south into the LH and toward the MBT between 10 and 6 Ma.

6. Conclusions

[57] Our results indicate that rapid crustal exhumation documented in a belt along the southern slopes of the Higher (or Greater) Himalaya have possibly been exhumed with similar rates to what has been observed in the western and eastern syntaxes, as well as in central Nepal during late Miocene until present day. More proximal and internal regions of the orogen (the LH and TH) experienced an order of magnitude lower exhumation rate during the same time. Major temporal variations in exhumation rate in the High Himalaya are spatially consistent in a 40–80 km wide belt along 200 km of strike of the area studied, and are insensitive to structural variations.

[58] Our main findings indicate that:

[59] 1. Major temporal variations in exhumation occurred in the early middle Miocene and at the Pliocene/Pleistocene transition, respectively. Most notably, minimum estimated exhumation rates for the internal and northern compartments of the High Himalaya, forming the hanging wall of the MCT, were highest (~3 mm a^{-1}) between ~23–19 Ma and (~2 mm a^{-1}) between 3 and 0 Ma, with a deceleration in rates (0.4–0.8 mm a^{-1}) noted between ~19–3 Ma.

[60] 2. Contemporaneously, in the footwall of the MCT to the south, we obtained consistently high exhumation rates

of 2–3 mm a^{-1} between 11 and 3 Ma and possibly longer, for Lesser Himalayan Crystalline rocks.

[61] 3. Although rainfall, relief, and specific stream power (proxies for modern erosion) in the Himalaya are among the highest globally, spatial correlations between calculated long-term exhumation rates and these proxies are poor. We interpret this poor correlation to be the consequence of either (1) temporal variation in erosion, which are possibly beyond the resolution of what thermochronometers are able to detect, (2) a lack of sensitivity to detect changes in cooling because of varying erosion in rapidly exhuming regions (>1 mm a^{-1}), and/or (3) that the thermochronometer samples in this region cooled under topographic conditions that only weakly resemble the present-day conditions. Consequently a strong correlation between long-term exhumation and relief or stream power could still exist in our study area, but is not resolvable with the thermochronometric data available in this study.

[62] 4. Our new AFT data improve constraints on the tectonic evolution of the Lesser Himalaya. They suggest that crystalline nappe emplacement and posttectonic regional thermal reequilibration happened prior to 12–10 Ma. It was followed by river incision and erosion-driven exhumation with average rates of ~1 mm a^{-1} since at least ~6 Ma until present.

Appendix A: Justification for 1-D Steady State Thermal Model

[63] Previous thermochronometer studies of the Himalaya have used numerical models of varying sophistication to interpret exhumation rates. *Whipp et al.* [2007] and *Huntington et al.* [2007] present two of the more advanced, 3-D, approaches where the effect of 3-D exhumation trajectories on sample cooling ages in Nepal is accounted for. Here we explain our rationale for using a 1-D thermal model to quantify exhumation rates.

[64] First, previous work indicates that low-temperature thermochronometer data have a decreased sensitivity to the exhumation pathway in rapidly eroding orogens. For example, *Whipp et al.* [2007] found a low sensitivity of AFT and $^{40}Ar/^{39}Ar$-wM cooling ages to lateral exhumation along thrusts [see *Whipp et al.*, 2007, Figure 8]. The reason for this is that exhumation rates, and thermal gradients, are sufficiently high that sample cooling histories are not integrated over a long enough distance to distinguish between lateral and vertical motion. Instead, *Whipp et al.* [2007] found that cooling ages are most sensitive to the vertical (1-D exhumation) component of the kinematic field. Thus, although useful information can be gleaned from 3-D models, in rapidly eroding regions such as the Himalaya, cooling ages are predominately sensitive to vertical (1-D) motion. This would not be the case for lateral motion of rocks in more slowly exhuming settings.

[65] Second, thermal transients are typically short-lived in rapidly eroding orogens. Previous studies have highlighted that transient denudation rates can result in temporal variations in thermal gradients and closure isotherm depths [e.g., *Mancktelow and Grasemann*, 1997]. However, the response time of the thermal field to variable denudation rates depends primarily on the magnitude and duration of changes in the denudation rate [e.g., *Reiners and Brandon*, 2006]. In general, the faster the exhumation rate is around which changes occur, the faster the response time is until the thermal field reaches a new thermal equilibrium. Relevant to our application of a steady state model we highlight that:

[66] 1. AFT age/elevation relationships from the High Himalaya are linear over the last 3–4 Ma (Figure 2), suggesting constant exhumation rates over this duration.

[67] 2. Application of the program RESPTIME [see *Ehlers et al.*, 2005; *Reiners and Brandon*, 2006] to Himalayan conditions simulated in this study suggests a rapid equilibration of the closure temperatures to a steady state thermal field following a step change in the exhumation rate. For example, the response time for the AFT closure isotherm to reach 90% of a new steady state depth is 1.2 ± 0.2 Ma for the change in exhumation rates suggest in this study of 0.5 to 2.0 mm a^{-1}. The response time was calculated using a 30-km-thick crust, thermal diffusivity between 28.6-50 km^2 Ma^{-1}, heat production rate between 11.5 and 34.4°C Ma^{-1}, and an initial thermal gradient of 45°C km^{-1}. The previous rapid response time suggests that for a change in exhumation rates prior to 3 Ma, (as suggested by linear AFT age-elevation relationships) the thermal field would be reequilibrated within ~1.2 Ma of this change. Thus, our interpretation of a change in rates from AFT ages that occurred ~2 Ma at 3 km depth suggests a minimal (<10%) influence of thermal transients on our interpretation of these data.

[68] Similarly, application of RESPTIME to quantify the duration of thermal transients between closure of the $^{40}Ar/^{39}Ar$-wM and ZFT used in this study also suggests a small effect on our interpretations. For example, for a decrease in rates from 3.0 to 0.5 mm a^{-1} ~19 Ma requires 8 ± 2 Ma before 80–90% of thermal equilibration to the new rate is achieved. This means that the decrease in rates between closure of the $^{40}Ar/^{39}Ar$-wM and ZFT data has a similarly low (<10–20%) effect on our interpretation of exhumation rates from ~13 Ma ZFT ages and ~19 Ma $^{40}Ar/^{39}Ar$-wM-ages.

[69] In summary, although thermal transients were likely present in the study area because of changes in rates, the rapid exhumation rates in the study area, and the range of ages used to calculate exhumation rates, suggest a small <10% to <20% effect of transients on our calculated rates.

Appendix B: Determination of Exhumation Rates

[70] The range of possible exhumation rates was determined by our best estimate considering varying thermophysical properties for the individual tectonomorphic provinces exhumed within the Himalaya. We used the model to identify the range of possible exhumation rates by varying model parameters such as the thermal conductivity and heat production, for all three thermochronometers (e.g., Figures S1, S2, and S3 within the auxiliary material accompanying this paper). The contours in Figures S1, S2, and S3 represent the predicted cooling ages of each thermochronometer system. Previously published and new thermal conductivity and heat production measurements for the LH, LHC, HHC, TH are summarized in Table S2 within the auxiliary material. Petrologic estimates of peak temperature and depth of metamorphics (i.e., HHC ~600–700°C, ~30 km depth) were used as the basal temperature

and depth boundary condition for the model. The individual plots of the model results presented in Figures S1, S2, and S3 took into consideration the range of plausible thermal conductivity and heat production values observed in this region. The white dashed boxes show the range of exhumation rates derived from the variability of cooling ages obtained within individual tectonomorphic units.

Appendix C: Thermal Conductivity Measurements

[71] Effective thermal conductivity (data table in auxiliary material accompanying this paper) was measured using the optical-scanning method on cut rock samples of at least 5 cm length and measured under dry laboratory conditions at ~20°C. The distribution of the thermal conductivity κ, and the coefficient of thermal heterogeneity both parallel and perpendicular to the metamorphic foliation was measured. The error of the measurement is <5% for thermal conductivities in the range of 0.2–50 W m^{-1} K^{-1} [*Popov and Pevzner*, 1994]. An effective porosity of 1% was assumed to be the typical value for all samples, yielding a ratio of the thermal conductivity of between water- and air-saturated rock of 1.03 [*Förster and Förster*, 2000].

[72] **Acknowledgments.** We are grateful to A. K. Jain and S. Singh from IIT Roorkee for their continued support and interest in our work in India. We thank Tashi Jigmet and D. Scherler for logistical support and assistance during fieldwork. A. Forster from GFZ Potsdam provided thermal conductivity measurements. J. Barnes and D. Whipp are thanked for comments on an earlier version of the paper. The paper was improved by constructive and thorough reviews by M. Bernet, A. Carter, P. Reiners, and associate editor Alex Densmore. We acknowledge financial support from the German Science Foundation (DFG) to R. Thiede (TH 1317/1–1) and M. Strecker (STR373/16–3) and support by the U.S. National Science Foundation to T. Ehlers (EAR-0724656).

References

Ahmad, T., N. Harris, M. Bickle, H. Chapman, J. Bunbury, and C. Prince (2000), Isotopic constraints on the structural relationships between the Lesser Himalayan series and the High Himalayan crystalline series, Garhwal Himalaya, *Geol. Soc. Am. Bull.*, *112*, 467–477, doi:10.1130/0016-7606(2000)112<0467:ICOTSR>2.3.CO;2.

Ahnert, F. (1970), Functional relationships between denudation, relief, and uplift in large mid-latitude basins, *Am. J. Sci.*, *268*, 243–263.

Bagnold, R. A. (1966), An approach to the sediment transport problem from general physics, *U.S. Geol. Surv. Prof. Pap.*, *422*, 11–137.

Bagnold, R. A. (1977), Bed load transport by natural rivers, *Water Resour. Res.*, *13*, 303–312, doi:10.1029/WR013i002p00303.

Barros, A. P., M. Joshi, J. Putkonen, and D. W. Burbank (2000), A study of the 1999 monsoon rainfall in a mountainous region in central Nepal using TRMM products and rain gauge observations, *Geophys. Res. Lett.*, *27*, 3683–3686, doi:10.1029/2000GL011827.

Beaumont, C., R. A. Jamieson, M. H. Nguyen, and B. Lee (2001), Himalayan tectonics explained by extrusion of a low-viscosity crustal channel coupled to focused surface denudation, *Nature*, *414*, 738–742, doi:10.1038/414738a.

Bernet, M., P. van der Beek, R. Pik, P. Huyghe, J. L. Mugnier, E. Labrin, and A. Szulc (2006), Miocene to recent exhumation of the central Himalaya determined from combined detrital zircon fission-track and U/Pb analysis of Siwalik sediments, western Nepal, *Basin Res.*, *18*(4), 393–412, doi:10.1111/j.1365-2117.2006.00303.x.

Bilham, R., K. Larson, and J. Freymuller (1997), GPS measurements of present-day convergence across the Nepal Himalaya, *Nature*, *386*, 61–64, doi:10.1038/386061a0.

Blythe, A., D. W. Burbank, A. Carter, K. Schmidt, and J. Putkonen (2007), Plio-Quaternary exhumation history of the central Nepalese Himalaya: 1. Apatite and zircon fission track and apatite [U-Th]/He analyses, *Tectonics*, *26*, TC3002, doi:10.1029/2006TC001990.

Bollinger, L., J. P. Avouac, O. Beyssac, E. J. Catlos, T. M. Harrison, M. Grove, B. Goffe, and S. Sapkota (2004), Thermal structure and exhumation history of the Lesser Himalaya in central Nepal, *Tectonics*, *23*, TC5015, doi:10.1029/2003TC001564.

Bookhagen, B., and D. W. Burbank (2006), Topography, relief, and TRMM-derived rainfall variations along the Himalaya, *Geophys. Res. Lett.*, *33*, L08405, doi:10.1029/2006GL026037.

Bookhagen, B., R. C. Thiede, and M. R. Strecker (2005), Late Quaternary intensified monsoon phases control landscape evolution in the NW Himalaya, *Geology*, *33*, 149–152, doi:10.1130/G20982.1.

Brandon, M. T., M. K. Roden-Tice, and J. I. Garver (1998), Late Cenozoic exhumation of the Cascadia accretionary wedge in the Olympic Mountains, northwest Washington State, *Geol. Soc. Am. Bull.*, *110*, 985–1009, doi:10.1130/0016-7606(1998)110<0985:LCEOTC>2.3.CO;2.

Braun, J. (2002), Estimating exhumation rate and relief evolution by spectral analysis of age-elevation datasets, *Terra Nova*, *14*, 210–214, doi:10.1046/j.1365-3121.2002.00409.x.

Burbank, D. W., A. E. Blythe, J. Putkonen, B. Pratt-Sitaula, E. Gabet, M. Oskin, A. Barros, and T. P. Ojha (2003), Decoupling of erosion and precipitation in the Himalayas, *Nature*, *426*, 652–655, doi:10.1038/nature02187.

Burchfiel, B. D., C. Zhileng, K. V. Hodges, L. Yuping, L. H. Royden, D. Changrong, and X. Jiene (1992), The South Tibetan detachment system, Himalayan orogen: Extension contemporaneous with and parallel to shortening in a collisional mountain belt, *Spec. Pap. Geol. Soc. Am.*, *269*, 1–41.

Burg, J. P., and G. M. Chen (1984), Tectonics and structural zonation of southern Tibet, *Nature*, *311*, 219–223, doi:10.1038/311219a0.

Burg, J. P., P. Nievergelt, F. Oberli, D. Seward, P. Davy, J. C. Maurin, Z. Z. Diao, and M. Meier (1998), The Namche Barwa syntaxis: Evidence for exhumation related to compressional crustal folding, *J. Asian Earth Sci.*, *16*, 239–252, doi:10.1016/S0743-9547(98)00002-6.

Caddick, M. J., M. J. Bickle, N. B. W. Harris, T. J. B. Holland, M. S. A. Horstwood, R. R. Parrish, and T. Ahmad (2007), Burial and exhumation history of a Lesser Himalayan schist: Recording the formation of an inverted metamorphic sequence in NW India, *Earth Planet. Sci. Lett.*, *264*, 375–390, doi:10.1016/j.epsl.2007.09.011.

Catlos, E. J., T. M. Harrison, M. Grove, A. Yin, M. J. Kohn, F. J. Ryerson, and P. LeFort (1997), Further evidence for late Miocene reactivation of the Main Central Thrust (Nepal Himalaya) and the significance of the MCT-1, *Eos Trans. AGU*, *78*, 651.

Cattin, R., and J. P. Avouac (2000), Modeling mountain building and the seismic cycle in the Himalaya of Nepal, *J. Geophys. Res.*, *105*, 13,389–13,407, doi:10.1029/2000JB900032.

Chambers, J. A., T. W. Argles, M. S. A. Horstwood, N. B. W. Harris, R. R. Parrish, and T. Ahmad (2008), Tectonic implications of Palaeoproterozoic anatexis and late Miocene metamorphism in the Lesser Himalayan Sequence, Sutlej Valley, NW India, *J. Geol. Soc.*, *165*, 725–737, doi:10.1144/0016-76492007/090.

Clift, P. D., and Z. Sun (2006), The sedimentary and tectonic evolution of the Yinggehai-Song Hong basin and the southern Hainan margin, South China Sea: Implications for Tibetan uplift and monsoon intensification, *J. Geophys. Res.*, *111*, B06405, doi:10.1029/2005JB004048.

Clift, P., C. Gaedicke, R. Edwards, J. I. Lee, P. Hildebrand, S. Amjad, R. S. White, and H. U. Schluter (2002), The stratigraphic evolution of the Indus Fan and the history of sedimentation in the Arabian Sea, *Mar. Geophys. Res.*, *23*, 223–245, doi:10.1023/A:1023627123093.

Clift, P. D., et al. (2008), Holocene erosion of the Lesser Himalaya triggered by intensified summer monsoon, *Geology*, *36*, 79–82, doi:10.1130/G24315A.1.

Copeland, P., and M. T. Harrison (1990), Episodic rapid uplift in the Himalaya revealed by $^{40}Ar/^{39}Ar$ analysis of detrital K-felspar and muscovite, Bengal fan, *Geology*, *18*, 354–359, doi:10.1130/0091-7613(1990)018<0354:ERUITH>2.3.CO;2.

Craddock, W. H., D. W. Burbank, B. Bookhagen, and E. J. Gabet (2007), Bedrock channel geometry along an orographic rainfall gradient in the upper Marsyandi River valley in central Nepal, *J. Geophys. Res.*, *112*, F03007, doi:10.1029/2006JF000589.

Dahlen, F. A., and J. Suppe (1988), Mechanics, growth, and erosion of mountain belts, in *Processes in Continental Lithospheric Deformation*, edited by S. P. Clark et al., *Spec. Pap. Geol. Soc. Am.*, *218*, 161–178.

Dahlen, F. A., J. Suppe, and D. Davis (1984), Mechanics of fold-and-thrust belts and accretionary wedges: Cohesive Coulomb wedge theory, *J. Geophys. Res.*, *89*, 10,087–10,101, doi:10.1029/JB089iB12p10087.

Davis, D., J. Suppe, and F. A. Dahlen (1983), Mechanics of fold-and-thrust belts and accretionary wedges, *J. Geophys. Res.*, *88*, 1153–1172, doi:10.1029/JB088iB02p01153.

DeCelles, P. G., G. E. Gehrels, J. Quade, T. P. Ojha, P. A. Kapp, and B. N. Upreti (1998), Neogene foreland basin deposits, erosional unroofing, and the kinematic history of the Himalayan fold-thrust belt, western Nepal, *Geol. Soc. Am. Bull.*, *110*, 2–21, doi:10.1130/0016-7606(1998)110<0002:NFBDEU>2.3.CO;2.

DeCelles, P. G., D. M. Robinson, J. Quade, T. P. Ojha, C. N. Garzione, P. Copeland, and B. N. Upreti (2001), Stratigraphy, structure, and tectonic evolution of the Himalayan fold-thrust belt in western Nepal, *Tectonics*, *20*, 487–509, doi:10.1029/2000TC001226.

Dettman, D. L., M. J. Kohn, J. Quade, F. J. Ryerson, T. P. Ojha, and S. Hamidullah (2001), Seasonal stable isotope evidence for a strong Asian monsoon throughout the past 10.7 m.y., *Geology*, *29*, 31–34, doi:10.1130/0091-7613(2001)029<0031:SSIEFA>2.0.CO;2.

Dettman, D. L., X. M. Fang, C. N. Garzione, and J. J. Li (2003), Uplift-driven climate change at 12 Ma: A long $\delta^{18}O$ record from the NE margin of the Tibetan Plateau, *Earth Planet. Sci. Lett.*, *214*, 267–277, doi:10.1016/S0012-821X(03)00383-2.

Dezes, P. J., J. C. Vannay, A. Steck, F. Bussy, and M. Cosca (1999), Synorogenic extension: Quantitative constraints on the age and displacement of the Zanskar shear zone (northwest Himalaya), *Geol. Soc. Am. Bull.*, *111*, 364–374, doi:10.1130/0016-7606(1999)111<0364:SEQCOT>2.3.CO;2.

Dodson, M. H. (1973), Closure temperature in cooling geochronological and petrological systems, *Contrib. Mineral. Petrol.*, *40*, 259–274, doi:10.1007/BF00373790.

Dumitru, T. A. (1993), A new computer-automated microscope stage system for fission-track analysis, *Nucl. Tracks Radiat. Meas.*, *21*, 575–580.

Dumitru, T. A. (2000), Fission-track geochronology, in *Quaternary Geochronology: Methods And Applications*, vol. 4, *AGU Reference Shelf*, edited by J. S. Noller et al., pp. 131–155, AGU, Washington, D. C.

Dunkl, I. (2002), Trackkey: A Windows program for calculation and graphical presentation of fission track data, *Comput. Geosci.*, *28*(1), 3–12.

Ehlers, T. A., and K. A. Farley (2003), Apatite (U-Th)/He thermochronometry: Methods and applications to problems in tectonic and surface processes, *Earth Planet. Sci. Lett.*, *206*, 1–14, doi:10.1016/S0012-821X(02)01069-5.

Ehlers, T. A., S. D. Willett, P. A. Armstrong, and D. S. Chapman (2003), Exhumation of the central Wasatch Mountains, Utah: 2. Thermokinematic model of exhumation, erosion, and thermochronometer interpretation, *J. Geophys. Res.*, *108*(B3), 2173, doi:10.1029/2001JB001723.

Ehlers, T. A., et al. (2005), Computational tools for low-temperature thermochronometer interpretation, *Rev. Mineral. Geochem.*, *58*, 589–622, doi:10.2138/rmg.2005.58.22.

England, P., P. Lefort, P. Molnar, and A. Pecher (1992), Heat-sources for tertiary metamorphism and anatexis in the Annapurna-Manaslu region central Nepal, *J. Geophys. Res.*, *97*, 2107–2128, doi:10.1029/91JB02272.

Förster, A., and H.-J. Förster (2000), Crustal composition and mantle heat flow: Implications from surface heat flow and radiogenic heat production in the Variscan Erzgebirge (Germany), *J. Geophys. Res.*, *105*, 27,917–27,938.

Fuchs, G. C. (1981), Geologic-tectonical map of the Himalaya (E 70–E 95/N 35–N 25), map, scale1:2,000,000, Geol. Bundesanst., Vienna.

Gaetani, M., and E. Garzanti (1991), Multicyclic history of the northern India continental margin (northwestern Himalaya), *Bull. Am. Assoc. Pet. Geol.*, *75*, 1427–1446.

Galbraith, R. F. (1981), On statistical models for fission-track counts, *J. Math. Geol.*, *13*, 471–478.

Galbraith, R. F., and G. M. Laslett (1993), Statistical models for mixed fission-track ages, *Nucl. Tracks Radiat. Meas.*, *21*, 459–470.

Gansser, A. (1964), *Geology of the Himalayas*, 289 pp., Interscience, London.

Garzanti, E., A. Baud, and G. Mascle (1987), Sedimentary record of the northward flight of India and its collision with Eurasia (Ladakh Himalaya, India), *Geodin. Acta*, *1*, 297–312.

Green, P. F. (1981), A new look at statistics in fission-track dating, *Nucl. Tracks Radiat. Meas.*, *5*, 77–86.

Grujic, D., M. Casey, C. Davidson, L. S. Hollister, R. Kundig, T. Pavlis, and S. Schmid (1996), Ductile extrusion of the Higher Himalayan Crystalline in Bhutan: Evidence from quartz microfabrics, *Tectonophysics*, *260*, 21–43, doi:10.1016/0040-1951(96)00074-1.

Grujic, D., I. Coutand, B. Bookhagen, S. Bonnet, A. Blythe, and C. Duncan (2006), Climatic forcing of erosion, landscape, and tectonics in the Bhutan Himalayas, *Geology*, *34*, 801–804, doi:10.1130/G22648.1.

Harrison, T. M., F. J. Ryerson, P. Le Fort, A. Yin, O. M. Lovera, and E. J. Catlos (1997), A late Miocene-Pliocene origin for the central Himalayan inverted metamorphism, *Earth Planet. Sci. Lett.*, *146*, 1–7, doi:10.1016/S0012-821X(96)00215-4.

Hilley, G. E., and M. R. Strecker (2004), Steady state erosion of critical Coulomb wedges with applications to Taiwan and the Himalaya, *J. Geophys. Res.*, *109*, B01411, doi:10.1029/2002JB002284.

Hodges, K. V. (2000), Tectonics of the Himalaya and southern Tibet from two perspectives, *Geol. Soc. Am. Bull.*, *112*, 324–350, doi:10.1130/0016-7606(2000)112<0324:TOTHAS>2.3.CO;2.

Hodges, K. V., R. R. Parrish, and M. P. Searle (1996), Tectonic evolution of the central Annapurna Range, Nepalese Himalayas, *Tectonics*, *15*, 1264–1291, doi:10.1029/96TC01791.

Hodges, K. V., J. M. Hurtado, and K. X. Whipple (2001), Southward extrusion of Tibetan crust and its effect on Himalayan tectonics, *Tectonics*, *20*, 799–809, doi:10.1029/2001TC001281.

Hodges, K. V., C. Wobus, K. Ruhl, T. Schildgen, and K. Whipple (2004), Quaternary deformation, river steepening, and heavy precipitation at the front of the Higher Himalayan ranges, *Earth Planet. Sci. Lett.*, *220*, 379–389, doi:10.1016/S0012-821X(04)00063-9.

Hoth, S., J. Adam, N. Kukowski, and O. Oncken (2006), Influence of erosion on the kinematics of bivergent orogens. Results from scaled sandbox-simulations, paper presented at Tectonics, Climate, and Landscape Evolution, Geol. Soc. of Am., Sioulin, Taiwan.

Hurford, A. J., and P. F. Green (1983), The zeta-age calibration of fission-track dating, *Isot. Geosci.*, *1*(4), 285–317.

Huntington, K. W., A. E. Blythe, and K. V. Hodges (2006), Climate change and late Pliocene acceleration of erosion in the Himalaya, *Earth Planet. Sci. Lett.*, *252*, 107–118, doi:10.1016/j.epsl.2006.09.031.

Huntington, K. W., T. A. Ehlers, K. V. Hodges, and D. M. Whipp (2007), Topography, exhumation pathway, age uncertainties, and the interpretation of thermochronometer data, *Tectonics*, *26*, TC4012, doi:10.1029/2007TC002108.

Huyghe, P., A. Galy, J.-L. Mugnier, and C. France-Lanord (2001), Propagation of the thrust system and erosion in the Lesser Himalaya: Geochemical and sedimentological evidence, *Geology*, *29*, 1007–1010, doi:10.1130/0091-7613(2001)029<1007:POTTSA>2.0.CO;2.

Huyghe, P., J. L. Mugnier, A. P. Gajurel, and B. Delcaillau (2005), Tectonic and climatic control of the changes in the sedimentary record of the Karnali River section (Siwaliks of western Nepal), *Isl. Arc, Deep Sea Trenches Back-Arc Basins*, *14*, 311–327, doi:10.1111/j.1440-1738.2005.00500.x.

Jain, A. K., D. Kumar, S. Singh, A. Kumar, and N. Lal (2000), Timing, quantification and tectonic modelling of Pliocene-Quaternary movements in the NW Himalaya: Evidence from fission track dating, *Earth Planet. Sci. Lett.*, *179*, 437–451, doi:10.1016/S0012-821X(00)00133-3.

Jamieson, R. A., C. Beaumont, S. Medvedev, and M. H. Nguyen (2004), Crustal channel flows: 2. Numerical models with implications for metamorphism in the Himalayan-Tibetan orogen, *J. Geophys. Res.*, *109*, B06407, doi:10.1029/2003JB002811.

Jamieson, R. A., C. Beaumont, M. H. Nguyen, and D. Grujic (2006), Provenance of greater Himalayan Sequence and associated rocks: Predictions of channel flow models, in *Channel Flow, Ductile Extrusion and Exhumation in Continental Collision Zones*, edited by R. D. Law et al., *Spec. Publ. Geol. Soc. London*, *268*, 165–182.

Knighton, A. D. (1998), *Fluvial Forms And Processes – A New Perspective*, 384 pp., Edward Arnold Ltd., London.

Koons, P. O. (1989), The topographic evolution of collisional mountain belts: A numerical look at the Southern Alps, New Zealand, *Am. J. Sci.*, *289*, 1041–1069.

Kutzbach, J. E., W. L. Prell, and W. F. Ruddiman (1993), Sensitivity of Eurasian climate to surface uplift of the Tibetan Plateau, *J. Geol.*, *100*, 177–190.

Lal, N., Y. D. Mehta, D. Kumar, A. Kumar, and A. K. Jain (1999), Cooling and exhumation history of the Mandi granite and adjoining tectonic units, Himachal Pradesh, and estimation of closure temperature from external surface of zircon, in *Geodynamic of the NW Himalaya*, edited by A. K. Jain and R. M. Manickavasagam, report, pp. 207–216, Gondwana Res. Group., Osaka, Japan.

Laslett, G. M., P. F. Green, I. R. Duddy, and A. J. W. Gleadow (1987), Thermal annealing of fission tracks in apatite: 2, A quantitative analysis, *Chem. Geol.*, *65*, 1–13, doi:10.1016/0009-2541(87)90189-6.

Lavé, J., and J. P. Avouac (2001), Fluvial incision and tectonic uplift across the Himalaya of Central Nepal, *J. Geophys. Res.*, *106*, 26,561–26,591.

Law, R. D., M. P. Searle, and L. Godin (Eds.) (2006), *Channel Flow, Ductile Extrusion and Exhumation in Continental Collision Zones*, *Spec. Publ. Geol. Soc. London*, *268*, 1–632.

Lefort, P. (1975), Himalayas - collided range - present knowledge of continental arc, *Am. J. Sci.*, *275*, 1.

Leopold, L. B., and T. Maddock (1953), Hydraulic geometry of streams and some physiographic implications, *U. S. Geol. Surv. Prof. Pap.*, *252*, 57.

Mancktelow, N. S., and B. Grasemann (1997), Time-dependent effects of heat advection and topography on cooling histories during erosion, *Tectonophysics*, *270*, 167–195, doi:10.1016/S0040-1951(96)00279-X.

Meigs, A., D. W. Burbank, and R. A. Beck (1995), Middle-late Miocene (pre-10 Ma) initiation of the Main Boundary Thrust in the western Himalaya, *Geology*, *23*, 423–426, doi:10.1130/0091-7613(1995)023<0423:MLMMFO>2.3.CO;2.

Molnar, P., and P. England (1990), Late Cenozoic uplift of mountain ranges and global climatic change: Chicken or egg?, *Nature*, *346*, 29–34, doi:10.1038/346029a0.

Montgomery, D. R., and M. T. Brandon (2002), Topographic controls on erosion rates in tectonically active mountain ranges, *Earth Planet. Sci. Lett.*, *201*, 481–489, doi:10.1016/S0012-821X(02)00725-2.

Montgomery, D. R., and K. B. Gran (2001), Downstream variations in the width of bedrock channels, *Water Resour. Res.*, *37*, 1841–1846, doi:10.1029/2000WR900393.

Naeser, C. W. (1979), Fission-track dating and geological annealing of fission tracks, in *Lectures in Isotope Geology*, edited by E. Jäger and J. C. Hunziker, pp. 154–169, Springer, New York.

Nelson, K. D., et al. (1996), Partially molten middle crust beneath southern Tibet: Synthesis of project INDEPTH results, *Science*, *274*, 1684–1688, doi:10.1126/science.274.5293.1684.

Pandey, M. R., R. P. Tandukar, J. P. Avouac, J. Lave, and J. P. Massot (1995), Interseismic strain accumulation on the Himalayan crustal ramp (Nepal), *Geophys. Res. Lett.*, *22*, 751–754, doi:10.1029/94GL02971.

Patriat, P., and J. Achache (1984), Indo-Asia collision chronology and its implications for crustal shortening and driving mechanisms of plates, *Nature*, *311*, 615–621, doi:10.1038/311615a0.

Popov, Y. A., and L. A. Pevzner (1994), Vertical variation in heat flow density and rock thermal properties along the scientific boreholes of Russia, paper presented at VIIth International Symposium on the Observation of the Continental Crust Through Drilling, Drill., Obs. and Sampling of the Earths Cont. Crust, Santa Fe, N. M.

Pratt, B., D. W. Burbank, A. Heimsath, and T. Ojha (2002), Impulsive alluviation during early Holocene strengthened monsoons, central Nepal Himalaya, *Geology*, *30*, 911–914, doi:10.1130/0091-7613(2002)030<0911:IADEHS>2.0.CO;2.

Pratt-Sitaula, B., D. W. Burbank, A. Heimsath, and T. Qjha (2004), Landscape disequilibrium on 1000–10,000 year scales Marsyandi River, Nepal, central Himalaya, *Geomorphology*, *58*, 223–241, doi:10.1016/j.geomorph.2003.07.002.

Prell, W. L., and J. E. Kutzbach (1992), Sensitivity of the Indian monsoon to forcing parameters and implications for its evolution, *Nature*, *360*, 647–652, doi:10.1038/360647a0.

Purdy, J. E., and E. Jaeger (1976), K-Ar ages on rock-forming minerals from the Central Alps, *Mem. Sci. Geol.*, *30*, 1–31.

Quade, J., T. E. Cerling, and J. R. Bowman (1989), Development of Asian monsoon revealed by marked ecological shift during latest Miocene in northern Pakistan, *Nature*, *342*, 163–166, doi:10.1038/342163a0.

Rahl, J. M., T. A. Ehlers, and B. A. van der Pluijm (2007), Quantifying transient erosion of orogens with detrital thermochronology from syntectonic basin deposits, *Earth Planet. Sci. Lett.*, *256*, 147–161, doi:10.1016/j.epsl.2007.01.020.

Ray, L., A. Bhattacharya, and S. Roy (2007), Thermal conductivity of Higher Himalayan Crystallines from Garhwal Himalaya, India, *Tectonophysics*, *434*, 71–79, doi:10.1016/j.tecto.2007.02.003.

Rea, D. K. (1993), Delivery of Himalayan sediment to the northern Indian Ocean and its relation to global climate, sea level, uplift, and seawater strontium, in *Synthesis of Results from Scientific Drilling in the Indian Ocean, Geophys. Monogr. Ser.*, vol. 70, edited by R. A. Duncan et al., pp. 387–402, AGU, Washington, D. C.

Reiners, P. W., and M. T. Brandon (2006), Using thermochronology to understand orogenic erosion, *Annu. Rev. Earth Planet. Sci.*, *34*, 419–466, doi:10.1146/annurev.earth.34.031405.125202.

Reiners, P. W., T. A. Ehlers, S. G. Mitchell, and D. R. Montgomery (2003), Coupled spatial variations in precipitation and long-term erosion rates across the Washington Cascades, *Nature*, *426*, 645–647, doi:10.1038/nature02111.

Reiners, P. W., T. A. Ehlers, and P. K. Zeitler (2005), Past, present, and future of thermochronology, in *Low-Temperature Thermochronology: Techniques, Interpretations, and Applications*, edited by P. W. Reiners and T. A. Ehlers, *Rev. Mineral. Geochem.*, *58*, 1–18.

Robinson, D. M., P. G. DeCelles, C. N. Garzione, O. N. Pearson, T. M. Harrison, and E. J. Catlos (2003), Kinematic model for the Main Central thrust in Nepal, *Geology*, *31*, 359–362, doi:10.1130/0091-7613(2003)031<0359:KMFTMC>2.0.CO;2.

Robinson, D. M., P. G. DeCelles, and P. Copeland (2006), Tectonic evolution of the Himalayan thrust belt in western Nepal: Implications for channel flow models, *Geol. Soc. Am. Bull.*, *118*, 865–885, doi:10.1130/B25911.1.

Roy, S., and R. U. M. Rao (2000), Heat flow in the Indian shield, *J. Geophys. Res.*, *105*, 25,587–25,604, doi:10.1029/2000JB900257.

Schaller, M., and T. A. Ehlers (2006), Limits to quantifying climate driven changes in denudation rates with cosmogenic radionuclides, *Earth Planet. Sci. Lett.*, *248*, 153–167, doi:10.1016/j.epsl.2006.05.027.

Schlup, M., A. Carter, M. Cosca, and A. Steck (2003), Exhumation history of eastern Ladakh revealed by Ar-40/Ar-39 and fission-track ages: The Indus River-Tso Morari transect, NW Himalaya, *J. Geol. Soc.*, *160*, 385–399, doi:10.1144/0016-764902-084.

Searle, M. P., S. R. Noble, A. J. Hurford, and D. C. Rex (1999), Age of crustal melting, emplacement and exhumation history of the Shivling leucogranite, Garhwal Himalaya, *Geol. Mag.*, *136*, 513–525, doi:10.1017/S0016756899002885.

Seeber, L., and V. Gornitz (1983), River profiles along the Himalayan arc as indicators of active tectonics, *Tectonophysics*, *92*, 335–367, doi:10.1016/0040-1951(83)90201-9.

Sorkhabi, R. B., E. Stump, K. A. Foland, and A. K. Jain (1996), Fission-track and $^{40}Ar/^{39}Ar$ evidence for episodic denudation of the Gangotri granites in the Garhwal Higher Himalaya, India, *Tectonophysics*, *260*, 187–199, doi:10.1016/0040-1951(96)00083-2.

Srivastava, P., and G. Mitra (1994), Thrust geometries and deep-structure of the Outer and Lesser Himalaya, Kumaon and Garhwal (India): Implications for evolution of the Himalayan fold-and-thrust belt, *Tectonics*, *13*, 89–109, doi:10.1029/93TC01130.

Stüwe, K., L. White, and R. Brown (1994), The influence of eroding topography on steady-state isotherms: Application to fission track analysis, *Earth Planet. Sci. Lett.*, *124*, 63–74, doi:10.1016/0012-821X(94)00068-9.

Summerfield, M. A., and N. J. Hulton (1994), Natural controls of fluvial denudation rates in major world drainage basins, *J. Geophys. Res.*, *99*, 13,871–13,883.

Thiede, R., B. Bookhagen, J. R. Arrowsmith, E. Sobel, and M. Strecker (2004), Climatic control on rapid exhumation along the Southern Himalayan Front, *Earth Planet. Sci. Lett.*, *222*, 791–806, doi:10.1016/j.epsl.2004.03.015.

Thiede, R. C., J. R. Arrowsmith, B. Bookhagen, M. O. McWilliams, E. R. Sobel, and M. R. Strecker (2005), From tectonically to erosionally controlled development of the Himalayan orogen, *Geology*, *33*, 689–692, doi:10.1130/G21483.1.

Thiede, R. C., J. R. Arrowsmith, B. Bookhagen, M. O. McWilliams, E. R. Sobel, and M. R. Strecker (2006), Dome formation and extension in the Tethyan Himalaya, Leo Pargil, NW-India, *Geol. Soc. Am. Bull.*, *118*, 635–650, doi:610.1130/B25872.25871.

Valdiya, K. S. (1980), The two intracrustal boundary thrusts of the Himalaya, *Tectonophysics*, *66*, 323–348, doi:10.1016/0040-1951(80)90248-6.

Vance, D., and N. Harris (1999), Timing of prograde metamorphism in the Zanskar Himalaya, *Geology*, *27*, 395–398, doi:10.1130/0091-7613(1999)027<0395:TOPMIT>2.3.CO;2.

Vannay, J. C., and B. Grasemann (2001), Himalayan inverted metamorphism and syn-convergence extension as a consequence of a general shear extrusion, *Geol. Mag.*, *138*, 253–276, doi:10.1017/S0016756801005313.

Vannay, J. C., B. Grasemann, M. Rahn, W. Frank, A. Carter, and V. Baudraz (2004), Miocene to Holocene exhumation of metamorphic crustal wedges in the Himalayan orogen: Evidence for tectonic extrusion coupled to fluvial erosion, *Tectonics*, *23*, TC1014, doi:10.1029/2002TC001429.

Wagner, G., and P. Van den Haute (1992), *Fission Track Dating*, 285 pp., Kluwer Acad., Dordrecht, Netherlands.

Wang, Q., et al. (2001), Present-day crustal deformation in China constrained by global positioning system measurements, *Science*, *294*, 574–577, doi:10.1126/science.1063647.

Whipp, D. M., and T. A. Ehlers (2007), Influence of groundwater flow on thermochronometer-derived exhumation rates in the central Nepalese Himalaya, *Geology*, *35*, 851–854, doi:10.1130/G23788A.1.

Whipp, D. M., T. A. Ehlers, A. E. Blythe, K. W. Huntington, K. V. Hodges, and D. W. Burbank (2007), Plio-Quaternary exhumation history of the central Nepalese Himalaya: 2. Thermokinematic and thermochronometer age prediction model, *Tectonics*, *26*, TC3003, doi:10.1029/2006TC001991.

Whipple, K. X., and B. J. Meade (2006), Orogen response to changes in climatic and tectonic forcing, *Earth Planet. Sci. Lett.*, *243*, 218–228, doi:10.1016/j.epsl.2005.12.022.

Willett, S. D. (1999), Orogeny and orography: The effects of erosion on the structure of mountain belts, *J. Geophys. Res.*, *104*, 28,957–28,982.

Wobus, C. W., K. V. Hodges, and K. X. Whipple (2003), Has focused denudation sustained active thrusting at the Himalayan topographic front?, *Geology*, *31*, 861–864, doi:10.1130/G19730.1.

Wobus, C., A. M. Heimsath, K. X. Whipple, and K. V. Hodges (2005), Active out-of-sequence thrust faulting in the central Nepalese Himalaya, *Nature*, *434*, 1008–1011, doi:10.1038/nature03499.

Zeitler, P. K., et al. (2001), Crustal reworking at Nanga Parbat, Pakistan: Metamorphic consequences of thermal-mechanical coupling facilitated by erosion, *Tectonics*, *20*, 712–728, doi:10.1029/2000TC001243.

Zhang, P., P. Molnar, and W. R. Downs (2001), Increased sedimentation rates and grain sizes 2–4 Myr ago due to the influence of climate change on erosion rates, *Nature*, *410*, 891–897, doi:10.1038/35073504.

Zhisheng, A., J. E. Kutzbach, W. L. Prell, and S. C. Porter (2001), Evolution of Asian monsoons and phased uplift of the Himalayan Tibetan Plateau since late Miocene times, *Nature*, *411*, 62–66, doi:10.1038/35075035.

B. Bookhagen, Department of Geography, University of California Santa Barbara, CA 94305, USA. (bodo@icess.ucsb.edu)

T. A. Ehlers, Department of Geological Sciences, University of Michigan, Ann Arbor, MI 48109, USA. (tehlers@umich.edu)

M. R. Strecker, Institut für Geowissenschaften, Universität Potsdam, D-14476 Potsdam-Golm, Germany. (strecker@geo.uni-potsdam.de)

R. C. Thiede, Geologisches Institut, ETH Zurich, CH-8092 Zurich, Switzerland. (rasmus@erdw.ethz.ch)